MARTIN MARIETTA ENERGY SYSTEMS LIBRARIES
3 4456 0137926 1

ORNL/TM-9904

ornl

OAK RIDGE NATIONAL LABORATORY

MARTIN MARIETTA

Protection of Spacecraft from Meteoroids and Orbital Debris

A. P. Fraas

OAK RIDGE NATIONAL LABORATORY
CENTRAL RESEARCH LIBRARY
CIRCULATION SECTION
4500N ROOM 175
LIBRARY LOAN COPY
DO NOT TRANSFER TO ANOTHER PERSON
If you wish someone else to see this report, send in name with report and the library will arrange a loan.

OPERATED BY
MARTIN MARIETTA ENERGY SYSTEMS, INC.
FOR THE UNITED STATES
DEPARTMENT OF ENERGY

Printed in the United States of America. Available from
National Technical Information Service
U.S. Department of Commerce
5285 Port Royal Road, Springfield, Virginia 22161
NTIS price codes—Printed Copy: A05 Microfiche A01

This report was prepared as an account of work sponsored by an agency of the United States Government. Neither the United States Government nor any agency thereof, nor any of their employees, makes any warranty, express or implied, or assumes any legal liability or responsibility for the accuracy, completeness, or usefulness of any information, apparatus, product, or process disclosed, or represents that its use would not infringe privately owned rights. Reference herein to any specific commercial product, process, or service by trade name, trademark, manufacturer, or otherwise, does not necessarily constitute or imply its endorsement, recommendation, or favoring by the United States Government or any agency thereof. The views and opinions of authors expressed herein do not necessarily state or reflect those of the United States Government or any agency thereof.

ORNL/TM-9904

Engineering Technology Division

PROTECTION OF SPACECRAFT FROM METEOROIDS AND ORBITAL DEBRIS

A. P. Fraas
Consultant

Date Published - March 1986

Prepared by the
OAK RIDGE NATIONAL LABORATORY
Oak Ridge, Tennessee 37831
operated by
MARTIN MARIETTA ENERGY SYSTEMS, INC.
for the
U.S. DEPARTMENT OF ENERGY
under Contract No. DE-AC05-84OR21400

MARTIN MARIETTA ENERGY SYSTEMS LIBRARIES
3 4456 0137926 1

ACKNOWLEDGMENTS

The writer acknowledges the assistance of the following people in obtaining recent information on the incidence of solid particles in orbital space, the damaging effects of impacts, and the efficacy of "bumpers."

R. E. English	NASA Lewis Research Center, Cleveland
S. V. Manson	NASA Headquarters, Washington, D.C.
J. Loria	NASA Headquarters, Washington, D.C.
B. G. Cour-Palais	NASA Space Center, Houston
D. J. Kessler	NASA Space Center, Houston
D. H. Humes	NASA Langley Research Center
G. Woodcock	Boeing Aerospace Co., Seattle
C. D. Miller	NASA Lewis Research Center (Retired)

In addition to their advice, these people supplied or suggested helpful reports and papers, which are included as references. Their assistance was invaluable and greatly appreciated.

K. M. Delker of the Martin Marietta Energy Systems, Inc. Y-12 Plant Library also provided valuable assistance by carrying out an extensive literature search by computer.

CONTENTS

	Page
ABSTRACT	1
1. INTRODUCTION	1
2. INCIDENCE OF METEOROIDS AND ORBITAL DEBRIS	3
3. DAMAGING EFFECTS OF METEOROIDS AND DEBRIS	11
4. PROTECTIVE BUMPERS	27
5. CONCLUSION	45
REFERENCES	47
APPENDIX	49

PROTECTION OF SPACECRAFT FROM METEOROIDS AND ORBITAL DEBRIS

A. P. Fraas

ABSTRACT

This report presents a review of information on the incidence of meteoroids and solid debris in orbital space, the damaging effects of these materials, and the principles that may be used to design protective shields for orbiting spacecraft. The report was prepared as part of a current Oak Ridge National Laboratory effort to develop and evaluate conceptual designs of space power systems.

---

1. INTRODUCTION

The possibility of a meteoroid puncture of the radiator (normally the largest and most vulnerable component of space power plants) has been of great concern since the initiation of work on space power plants. A substantial amount of experimental and analytical work was carried out between 1959 and 1970 (Refs. 1–6) which culminated in the design criteria presented in Refs. 4 and 5. Little attention was given to the problem in the 1970s, but there has been renewed interest during the past 2 years, for example, the studies included in Refs. 7 and 8 with which the writer was associated. During these latter studies, a brief review indicated that developments since 1970 have been consistent with the criteria given in Refs. 4 and 5, except that so much spacecraft debris has been accumulating in near-earth orbits that it now represents a much greater hazard than meteoroids of natural origin.[9-12] In view of these changes, this document was prepared to provide fairly comprehensive background information that will give perspective to these problems as well as provide information needed in the current Oak Ridge National Laboratory (ORNL) effort on space power plant design, evaluation, and development.

2. INCIDENCE OF METEOROIDS AND ORBITAL DEBRIS

ORNL meteorite damage studies performed in the early 1960s[2,3] were based on data for the incidence of meteoroids as a function of particle size provided by F. L. Whipple of the Smithsonian Astrophysical Laboratory. Subsequent data have generally confirmed these estimates for meteoroids of small size but show a lower incidence for those of large size, for example, a factor of ten lower incidence of meteoroids with masses of ~1 g. This difference is shown graphically in Fig. 1 where the data from Ref. 1 is superimposed on the current National Aeronautics and Space Administration (NASA) reference design curve from Ref. 4 that was first recommended in 1969. D. J. Kessler of NASA confirmed that the experimental data accumulated through 1985 show that the incidence of extraterrestrial meteoroids is within a factor or two of the NASA reference design curve in Fig. 1, except in the fine dust particle size range. Kessler states that meteoric particles of size less than 10^{-12} g, called beta meteoroids, exhibit a space density that results in an incidence increase of up to ten times the values taken from Fig. 1. Evidently the curve in Fig. 1 should continue further upward to the left as a straight line before leveling off. While this modification is important with regard to the erosion of optical surfaces (noticeable deterioration occurring over a few months), these particles are too light and the consequent erosion rate too low to damage most spacecraft surfaces.

The cumulative influx of meteoroids is less for higher orbits because of the reduced tendency of the earth's gravitational field to concentrate the meteoric material. This effect is shown in Fig. 2.

The velocity of meteoroids varies widely. Geocentric meteoroid velocities have been observed in a range from ~10 to ~75 km/s, with a high probability that the velocities will range from 10 to 30 km/s. The meteoroid velocity distribution is shown in Fig. 3.

It became evident in the late 1970s that spacecraft debris in low earth orbits was becoming a more serious threat than extraterrestrial meteoroids.[9-12] Figure 4 depicts a 1978 estimate of the problem. According to Kessler, however, the data available by early 1985 indicate that the incidence of this debris in the size range below a few

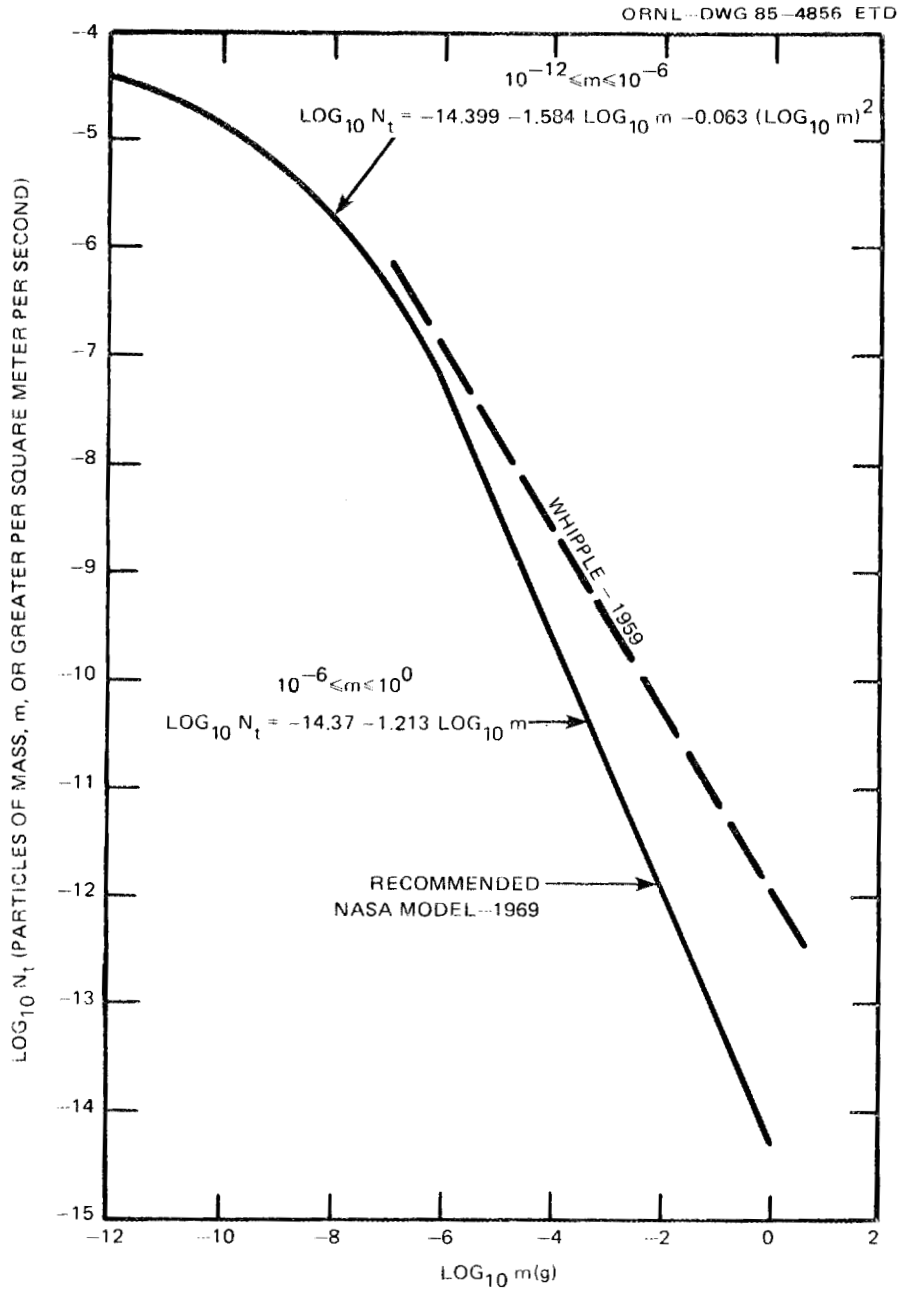

Fig. 1. Average cumulative flux of extraterrestrial meteoroids with greater than given mass in near-earth orbits. Source: B. G. Cour-Palais, *Meteoroid Environment Model — 1969 (Near Earth to Lunar Surface)*, NASA Space Vehicle Design Criteria (Environment), NASA SP-8013, National Aeronautics and Space Administration, 1969.

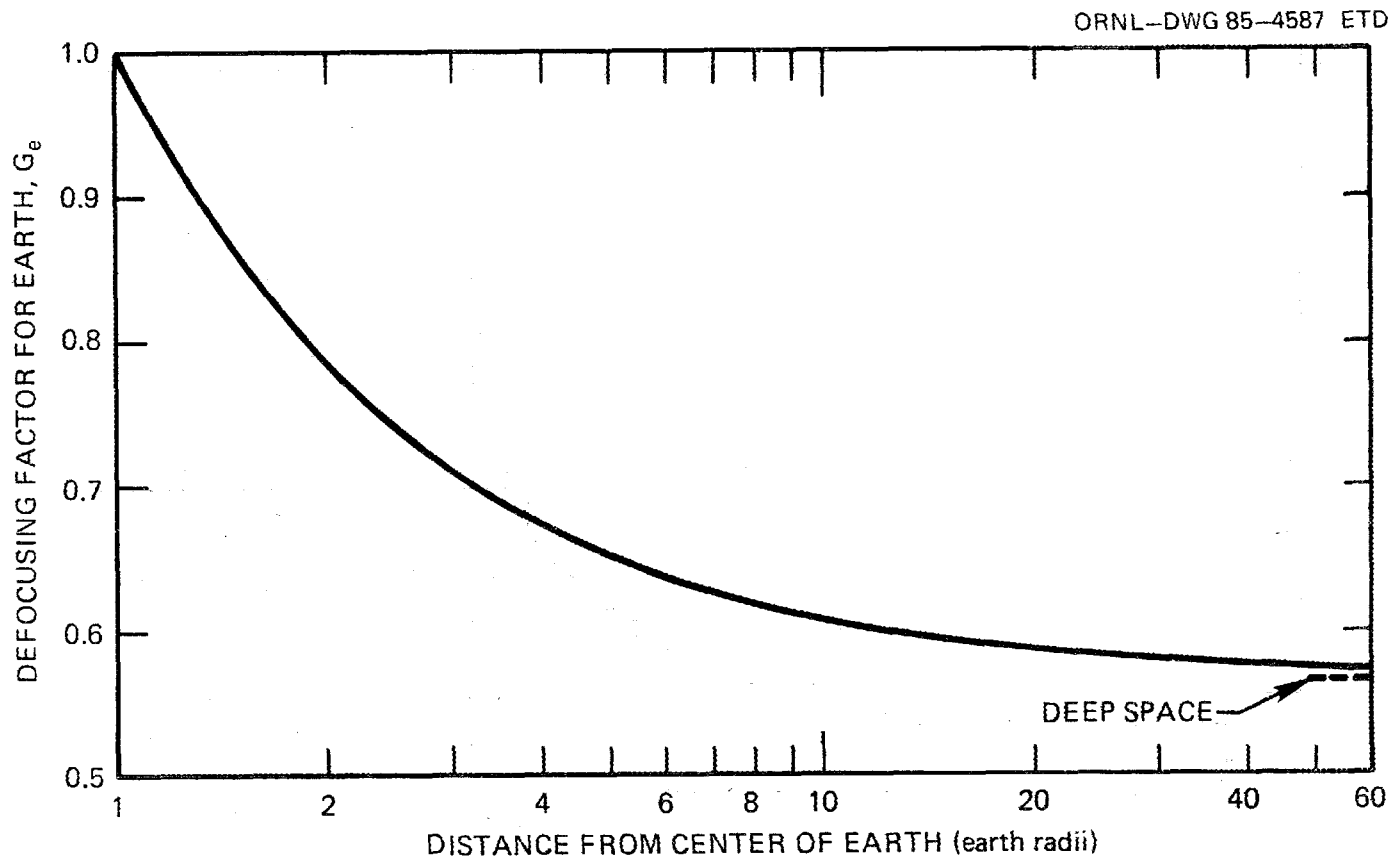

Fig. 2. Defocusing factor caused by earth's gravity for average meteoroid velocity of 20 km/s. Source: B. G. Cour-Palais, *Meteoroid Environment Model — 1969 (Near Earth to Lunar Surface)*, NASA Space Vehicle Design Criteria (Environment), NASA SP-8013, National Aeronautics and Space Administration, 1969.

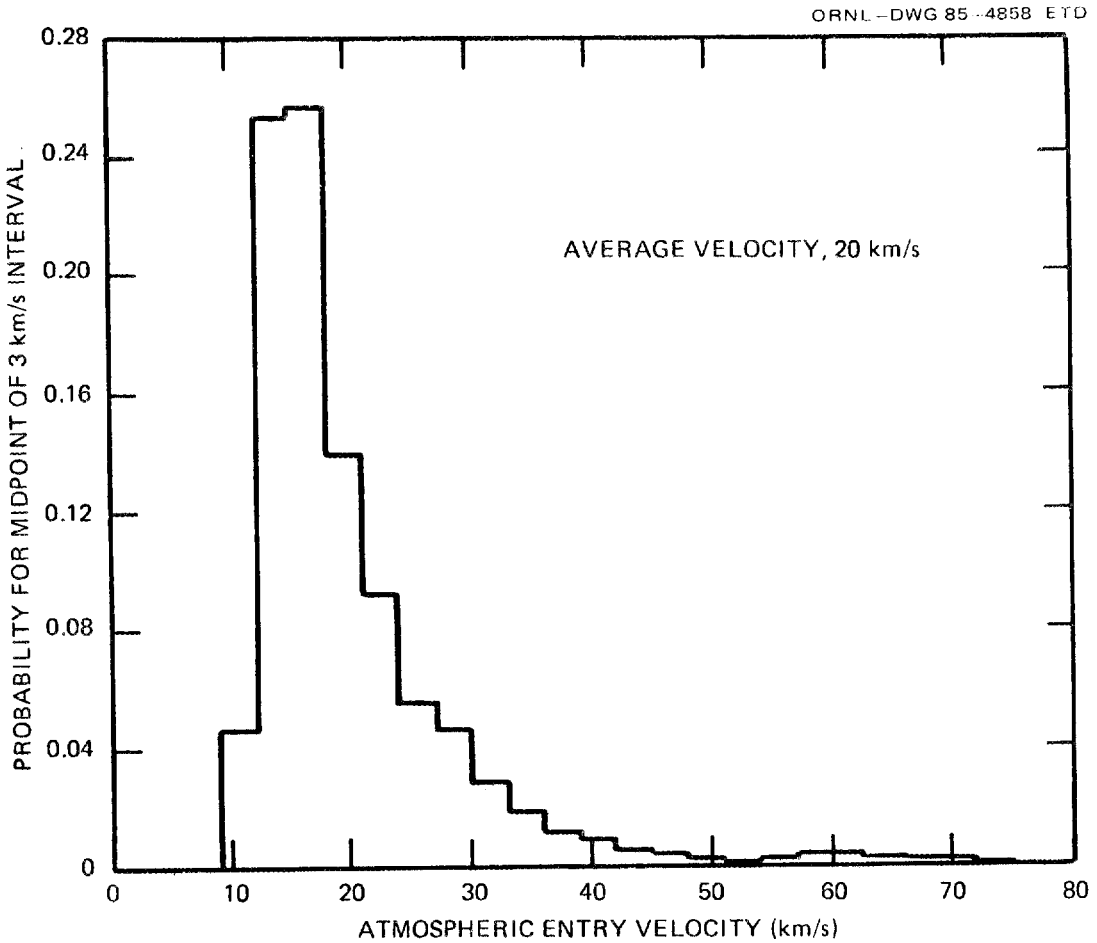

Fig. 3. Probability distribution for velocities of meteoroids entering earth's atmosphere. Source: B. G. Cour-Palais, *Meteoroid Environment Model — 1969 (Near Earth to Lunar Surface)*, NASA Space Vehicle Design Criteria (Environment), NASA SP-8013, National Aeronautics and Space Administration, 1969.

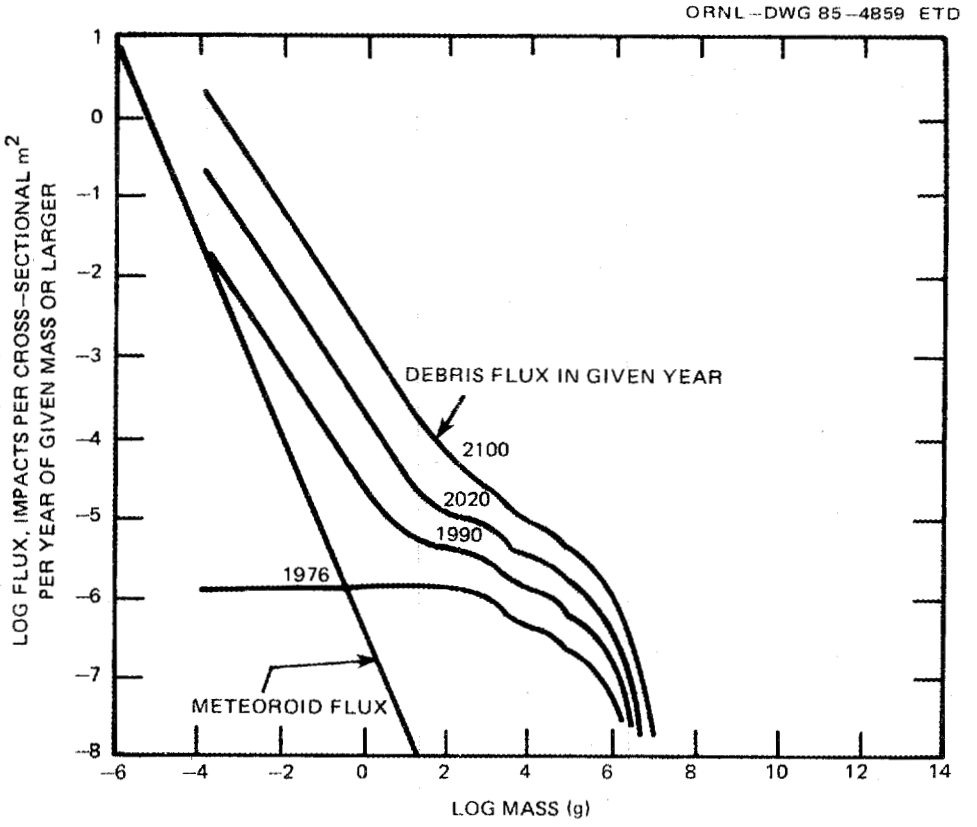

Fig. 4. NASA 1978 estimates of the flux of solid debris that would occur through year 2100 at altitudes between 700 and 1200 km. Source: D. J. Kessler and B. G. Cour-Palais, "Collision Frequency of Artificial Satellites: The Creation of a Debris Belt," *J. Geophys. Res.* 83 (A6), 2637-46 (June 1, 1978).

centimeters is increasing at a rate much greater than projected in 1978 and has already reached the level predicted for 1995 (see Fig. 4). One such set of data was presented as a result of a recent study conducted by the Massachusetts Institute of Technology's Lincoln Laboratory, which employed optical telescopes to look for objects in the size range above 1 cm.[13]

Another set of data showing a high incidence of spacecraft debris is emerging from the current examination of the Solar Max Satellite, which was removed from low earth orbit in April 1984 using the space shuttle. An ~2.5-m^2 sample of multilayered thermal insulation has provided an abundance of solid particle impact information. The outer layer is 0.05-mm-thick aluminum foil backed up with 17 layers of Kapton, each with a very thin coating of aluminum reflective insulation. The total thickness of this insulation configuration is ~0.25 mm. A microscopic examination revealed that many tiny craters in the outer layer of the aluminum were made by the impaction of flakes of paint. One incident particle of unknown origin penetrated the outer layer of aluminum leaving a 0.9-mm-diam hole, and continued through all 17 layers of insulation. A microscopic study of the particles trapped in the thermal insulation will yield valuable statistical data on the character of the fine particles encountered. Note that the relative velocity at the time of impact was generally much lower for orbiting spacecraft debris than for extraterrestrial particles. This could result in the energy released on impact not being sufficient to vaporize the incident particle.

The Long Duration Experiment Facility is a 14-ft-diam, 30-ft-long satellite weighing 8000 lb on which 1008 experimental trays are mounted to collect data on the incidence, chemical composition, and isotopic concentration of both meteoric material and spacecraft debris. This system was placed into orbit by a space shuttle in April 1984 and was scheduled to be retrieved during a space shuttle flight in March 1985. John Loria of NASA is responsible for the program and stated that the satellite will remain in orbit for an additional year because the retrieval flight was canceled. An additional year will be required subsequent to retrieval to analyze and report the information obtained.

Two NASA projects designed to yield further data on the incidence of spacecraft debris in low earth orbit are proposed. The first will employ two telescopes of about 30-cm aperture, which will be mounted at opposite ends of the space shuttle to permit triangulation measurements of both position and velocity of the particles observed. Data will be accumulated continuously over the 1-week flight. The experiment will avoid the limitations imposed by air aberration in optical observations that are ground-based and should provide good statistical data on orbiting particles in the size range from 0.1 to 1 cm (the size range of greatest interest in space power plant design). A proposed follow-on project will involve a similar experiment mounted on an orbiting satellite designed to accumulate data for about 1 year. Kessler estimates that this latter experiment will be launched in about 10 years.

3. DAMAGING EFFECTS OF METEOROIDS AND DEBRIS

Systematic analysis and experiments on the penetration of ductile plates by high velocity projectiles began with classic studies carried out by Krupp Industries in Germany over a century ago. Comparative experiments in Krupp machine shops revealed that the energy required to mechanically punch a hole in a steel plate was equal to the product of the ultimate shear strength of the plate material, the area of the wall of the hole punched, and the thickness of the plate. Krupp's ballistics tests showed that the same basic relation applied; that is, the loss in kinetic energy of the projectile was essentially equal to the product of the ultimate strength of the plate, the plate thickness, and the area of the wall of the hole punched by the projectile. This relation was found to give good correlation of experimental data for a wide range of projectile calibers and velocities and a wide range of armor plate alloys.

The muzzle velocity of the Krupp guns of that day was far below the sonic velocity in steel. Work performed more recently has shown that the mechanics of the impact event are quite different when the projectile velocity exceeds the sonic velocity of the target material. This situation is termed the "hypervelocity impact" regime, where the impact pressure so far exceeds the strength of the target material that it behaves as if it were a liquid. The damage from hypervelocity impact is spread over a much larger area of the target surface and takes the form of a hemispherical crater in sufficiently thick targets. While the crater formed has a diameter four or more times the projectile diameter, the depth of penetration for velocities immediately above the speed of sound in the target material might be only 25% of that for velocities that are just a little lower than the sonic velocity in the target material because the penetration mechanisms are completely different for these two regimes. For subsonic velocities in the target material, the projectile momentum goes into punching a hole about the diameter of the projectile, whereas in the course of a hypersonic impact, both the projectile and target material in the impact zone are liquified or vaporized and blasted away from the target by a violent pressure wave. The effect is much like that of a liquid droplet falling into a pool of

water except that a crater remains in the solid instead of being filled in by returning liquid.

Target penetration tests in the hypersonic regime can be accomplished either by using very high velocity projectiles or by using target materials with relatively low acoustic velocity. Considering that projectile velocities for a high-powered rifle rarely exceed 1000 m/s and this is only 20% of the sonic velocity in steel, it is easy to understand why the latter approach was most often taken. Tests in the hypervelocity regime are most easily accomplished with a target material such as lead, which has a sonic velocity of 1250 m/s as compared with 5100 m/s for aluminum and 5160 m/s for iron. Copper provides an intermediate candidate with a velocity of sound of 3700 m/s. Figure 5 shows a section through a hemispherical crater formed in a lead target by the hypervelocity impact of a 1.0-cm aluminum sphere at a velocity of 2020 m/s (6630 ft/s). The crater diameter is 4.2 cm, and the depth is 1.8 cm, or about half the crater diameter. A fairly high rim was formed around the edge of the crater because of the ductility of the target material. Proportionally, a much greater rim is produced than is seen around moon craters or the large meteor crater in Arizona, which were formed in brittle rock. The ductile metal flows plastically in regions where the stresses fall between the yield point and the ultimate shear stress. Considerable testing[14-18] performed with a wide variety of projectile materials and sizes, target materials, and projectile velocities, has yielded results consistent with those sketched in Fig. 5.

Valuable insights into the behavior of the material in the impact zone have been obtained from a computer analysis described in Ref. 19. Figure 6 shows four stages in the course of events of an impact of an aluminum ball on a thin aluminum plate at 7500 m/s. The small arrows shown in the figure are velocity vectors that indicate the movement of material in the impact zone at each particular point in time. The distribution of mass, axial momentum, and kinetic energy of the debris ejected from the impact zone is presented in Fig. 7. A comparison of similar results for projectile velocities of 7.5 and 15 km/s is presented in Fig. 8. The bulk of debris in low earth orbits that might impact on space power plants will impact at velocities bracketed by the projectile velocities in this figure.

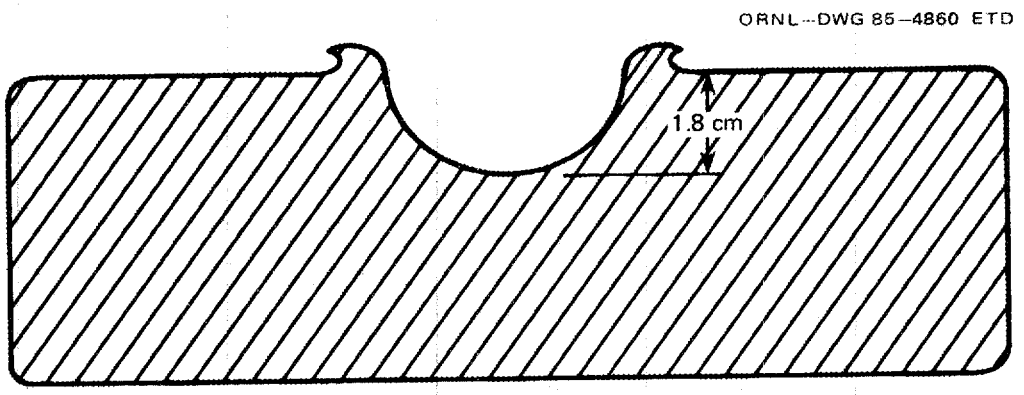

Fig. 5. Section through lead target showing crater left by impact of 1.0-cm-diam aluminum projectile striking at 2020 m/s (6630 ft/s). (Test by R. J. Eichelberger, Ballistics Research Laboratory, Aberdeen, MD).

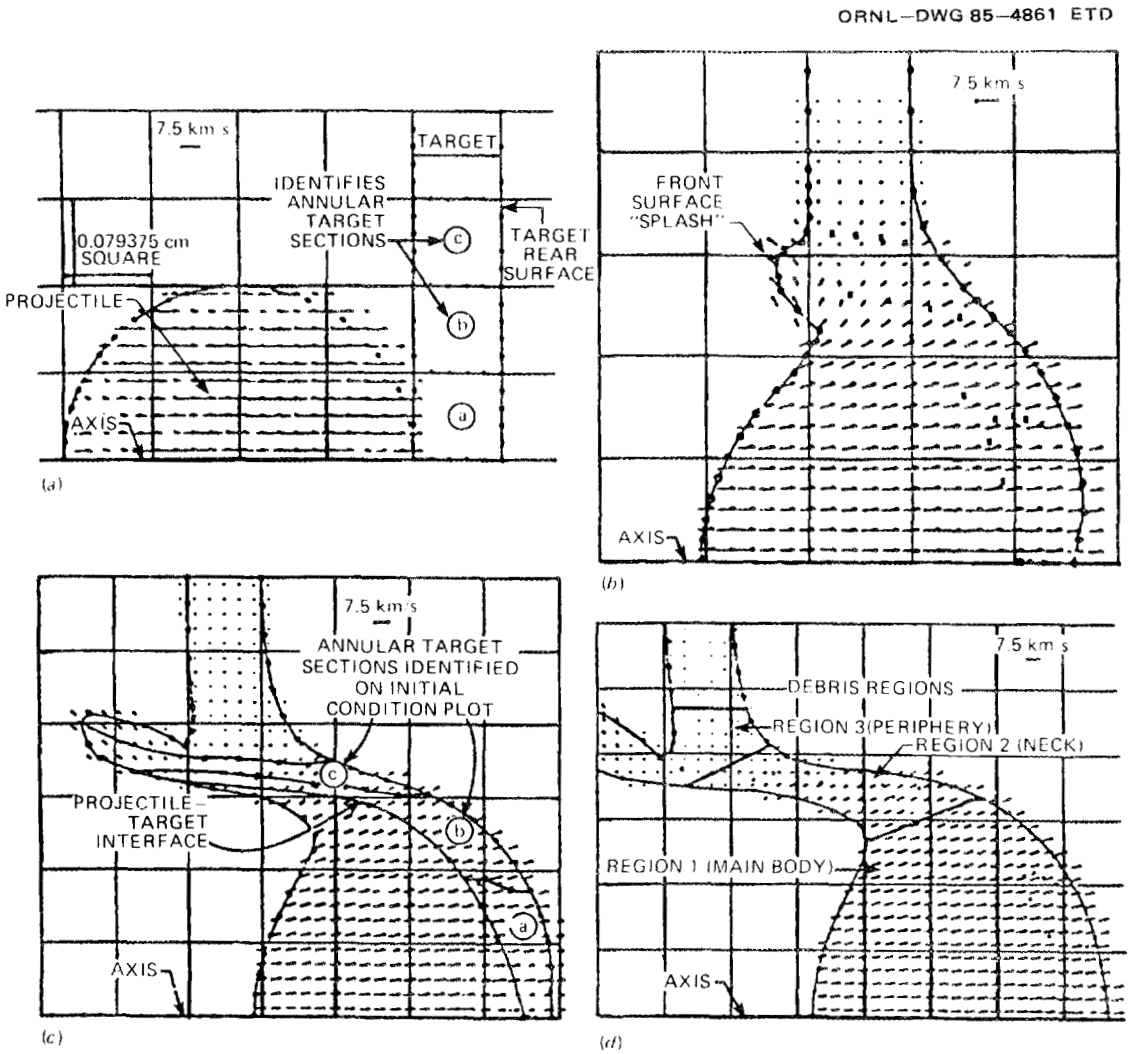

Fig. 6. Calculated velocity fields resulting from impact of an aluminum ball with velocity of 7.5 km/s on thin aluminum plate. (*a*), (*b*), (*c*), and (*d*) show, respectively, cross section of the materials and velocity vectors at impact and at periods of 0.12, 0.32, and 0.80 μs after impact. Source: M. H. Wagner and K. H. Kreyenhagen, "Review of the Hydro-Elastic-Plastic Code Analyses as Related to the Hypervelocity Particle Impact Hazard," *Proceedings of The Comet Halley Micrometeoroid Hazard Workshop*, Noordwijk, Netherlands, 18–19 April, 1979, European Space Agency, ESA-SP-153.

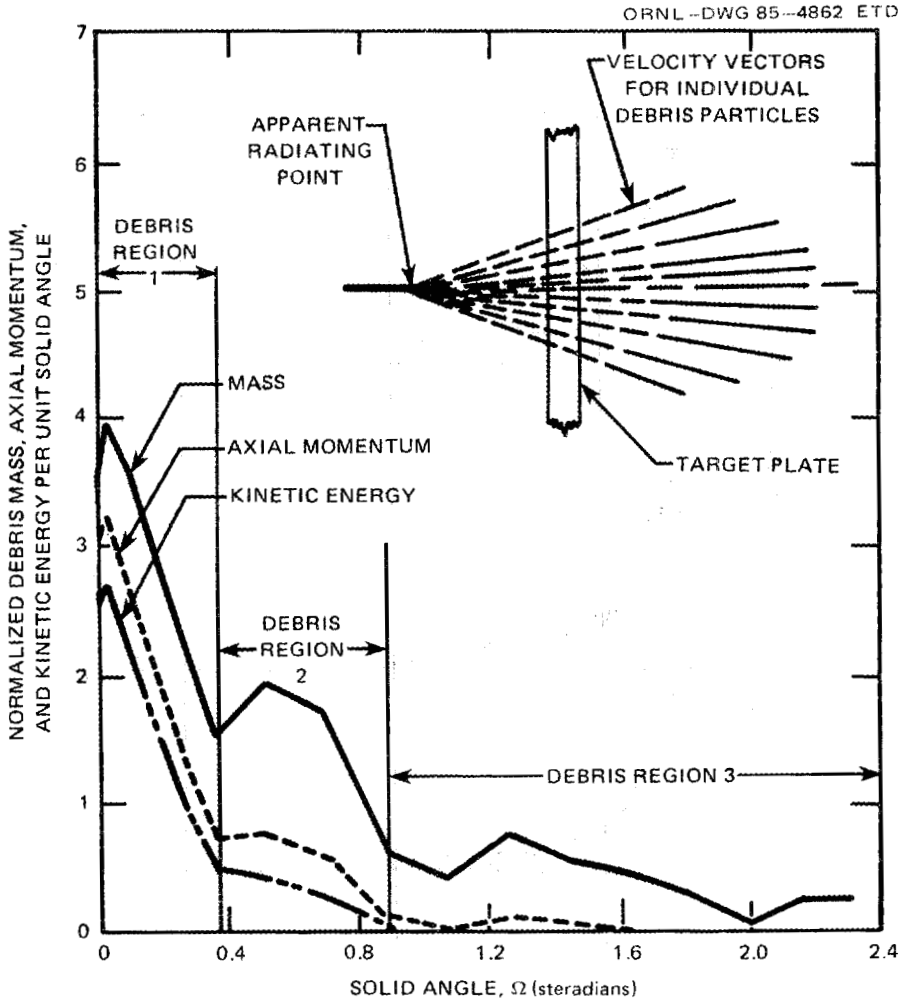

Fig. 7. Distribution of mass, axial momentum, and kinetic energy of debris ejected from impact of aluminum ball with velocity of 7.5 km/s on thin aluminum plate. Source: M. H. Wagner and K. H. Kreyenhagen, "Review of the Hydro-Elastic-Plastic Code Analyses as Related to the Hypervelocity Particle Impact Hazard," *Proceedings of The Comet Halley Micrometeoroid Hazard Workshop*, Noordwijk, Netherlands, 18–19 April, 1979, European Space Agency, ESA-SP-153.

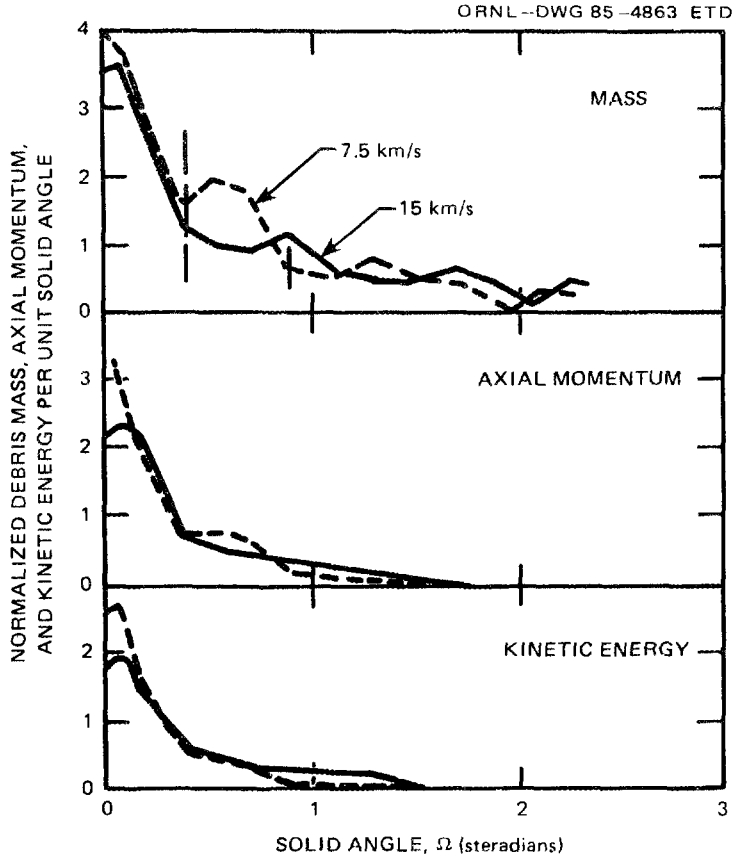

Fig. 8. Comparison of computed properties of debris ejected from impacts at 7.5 and 15 km/s. Source: M. H. Wagner and K. H. Kreyenhagen, "Review of the Hydro-Elastic-Plastic Code Analyses as Related to the Hypervelocity Particle Impact Hazard," *Proceedings of The Comet Halley Micrometeoroid Hazard Workshop*, Noordwijk, Netherlands, 18–19 April, 1979, European Space Agency, ESA-SP-153.

Computer calculations, such as those shown in Fig. 6, disclose that enormous pressures are developed at the instant of impact. The heating associated with the adiabatic compression of the material in the impact zone may be sufficient to melt or even vaporize part or all of the projectile and/or target material in the zone. Data presented in Ref. 19 show the impact pressure as a function of velocity for stoney projectiles with three densities in collision with two target materials, aluminum and steel. Plots of these data are shown in Fig. 9, along with the velocity regions where melting and vaporization will occur if half the kinetic energy in the projectile is converted into heat in the projectile material. The lower limit for each region represents the velocity level at which melting or vaporization would be initiated, while the upper limit indicates the level at which complete melting or vaporization would take place.

An important failure mode is found for target plate thicknesses intermediate between the thick plate considered in Fig. 5 and the thin plate of Fig. 6. In this intermediate region the shock wave reflected from the rear surface of the target as a rarefaction wave may induce such severe tensile stresses that substantial pieces may spall from the rear face, leaving a relatively large diameter shallow crater. Depending on the plate material and thickness, fissures may extend through the region between the hemispherical crater on the front face and the spalled cavity on the rear face of the plate. Consequently, extra thickness must be provided in the design of the wall of a system that must withstand a given impact threat and remain leaktight.

Because of the great variety of properties of projectile and target materials, it has not yet been possible to correlate them all on a purely theoretical basis. Efforts to rationalize empirical correlations have followed three different courses. One course advocated by Bjork in 1960,[20] was based on the premise that the volume of the crater produced in thick targets is proportional to the momentum of the incident projectile; thus, the penetration would vary as the cube root of the momentum. After allowing a factor of 1.5 to determine the thickness for incipient penetration and an additional term to allow for variations in the projectile density, Bjork proposed the following relation for the penetration of steel targets:

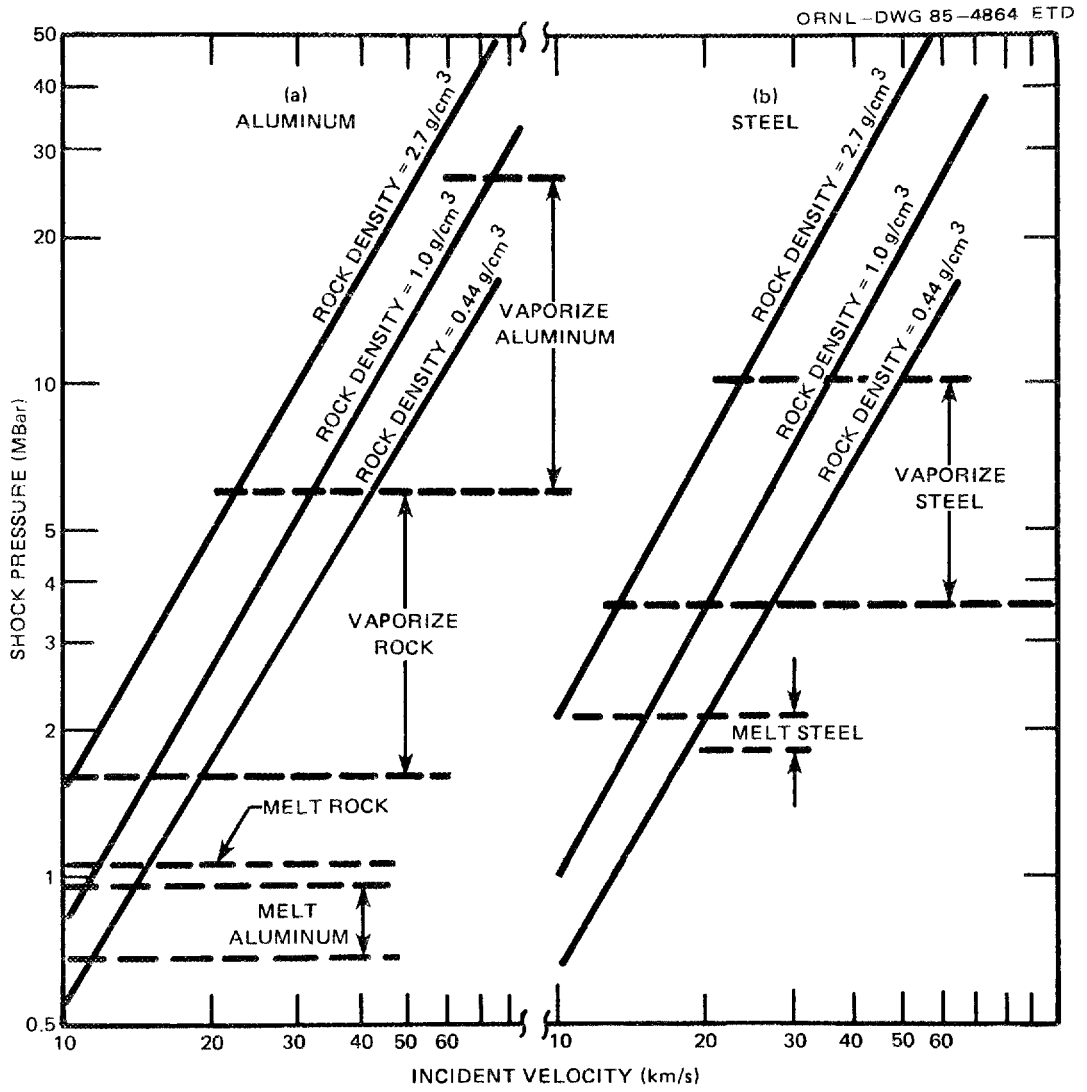

Fig. 9. Shock pressures as function of projectile velocity for stoney projectiles impacting on aluminum and steel (data from Ref. 19). The effects of conversion of half the kinetic energy in the incident projectile into heating of the projectile material are also shown.

$$t_s = 0.909\ (m_p\ V)^{1/3}\ (\rho_p/7.86)^{0.3}\ , \tag{1}$$

where

t_s = thickness for incipient penetration of steel, cm;

m_p = mass of projectile, g;

V = projectile velocity, km/s;

ρ_p = projectile density, g/cm^3.

This relation was used to estimate the thickness of the armor for protection of radiators in the ORNL designs of the early 1960s.

Various authorities (e.g., R. L. Eichelberger and J. H. Kineke of the Ballistics Research Laboratory at Aberdeen) have favored making the crater volume proportional to the kinetic energy of the projectile. Following this approach, Eq. (2) from a recent paper by Kineke[21] can be employed and rearranged to give an explicit expression for the target thickness for incipient penetration. Using the same symbols and units as in Eq. (1) gives the following:

$$t_s = 1020\ \rho_t^{-1/3}\ \sigma_t^{-1/3}\ m_p^{1/3}\ V^{2/3}\ , \tag{2}$$

where

σ_t = ultimate strength of the target material, Pa (e.g., 3.76×10^8 for aluminum and 1.97×10^9 for stainless steel)

Note that this equation is similar to Eq. (1), except that the thickness of the armor varies as the two-thirds power of the projectile velocity, and the ultimate strength of the target material is included as a major factor.

A third relation proposed by Fish and Summers at the Seventh Hypervelocity Impact Symposium has been widely used.[16] This empirical equation is similar to Eq. (2), but the exponents were modified to obtain a better fit to a wide variety of test data, and terms were added to include the effects of the density and ductility of the target material. This modification yielded the following relation:

$$t_s = \frac{0.816\ \rho_p^{0.418}\ m_p^{0.352}\ V^{0.875}}{\varepsilon_t^{1/18}\ \rho_t^{1/2}}\ , \tag{3}$$

where

ε_t = ductility of target material, %;

ρ_t = density of target material, g/cm^3.

Other symbols are the same as for Eq. (1).

A review of these and other empirical relations was performed at NASA (see Ref. 18) leading to the selection of Eq. (4) [which is very similar to Eq. (3)] to estimate target thickness for incipient penetration.

$$t_s = K_1\ m_p^{0.352}\ \rho_p^{0.167}\ V^{0.875}\ , \tag{4}$$

where the symbols are as defined previously, and K_1 depends on the physical properties of the target. Typical values for K_1 are presented in Table 1. Note that the effects of the density, ductility, and ultimate strength of the target material are included in K_1 for Eq. (4).

Examination of Eq. (4) and Table 1 reveals that the thickness of the armor for incipient penetration is mainly a function of the projectile mass and velocity and is relatively insensitive to the choice of material for the region of interest in space power plant design. In view of this, Table 2 and Fig. 10 present calculated thicknesses of a typical material (2024-T3 aluminum alloy) required to protect against penetration by meteoroids having a typical density of 0.5 g/cm^3. Table 3 provides correction factors for use with Fig. 10 to obtain the corresponding thicknesses for other combinations of projectile and target materials.

Equations (1)–(4) differ significantly, but the extent to which these differences affect the calculated thickness of the armor is not explicitly clear. To investigate this matter, Fig. 11 was prepared for a representative set of conditions (1.0-g meteoroids, having a density of 0.5 g/cm^3, striking a 2024-T3 aluminum target). Note that the spread is about ±50% and that Eq. (4) gives some of the higher values for the armor thicknesses. For this reason it should be considered one of the more conservative approaches. In appraising Fig. 11, it seems likely

Table 1. Constants for threshold penetration of a single plate at 25°C

Material	K_1	Basis
Aluminum alloys		
2024-T3, 2024-T4	0.54	Visual
7075-T6, 6061-T6	0.57	Pressure
Stainless steels		
AISI 304, AISI 316	0.32	Pressure
17 • 4 PH annealed	0.38	Pressure
Magnesium lithium		
LA 141-A	0.80	Pressure
Niobium alloys		
Nb-1Zr	0.34	Pressure

Table 2. The effects of meteoroid mass and relative impact velocity on the thickness, tm, of aluminum alloy targets for threshold penetration

	Thickness, cm			
Relative velocity, km/s	5	10	30	50
Meteroid mass, g				
1.000	2.08	3.81	9.95	15.6
0.100	0.92	1.69	4.43	6.92
0.010	0.41	0.75	1.97	3.08
0.001	0.18	0.33	0.88	1.37

Meteoroid density = 0.5 g/cm^3; K_1 for aluminum = 0.57.

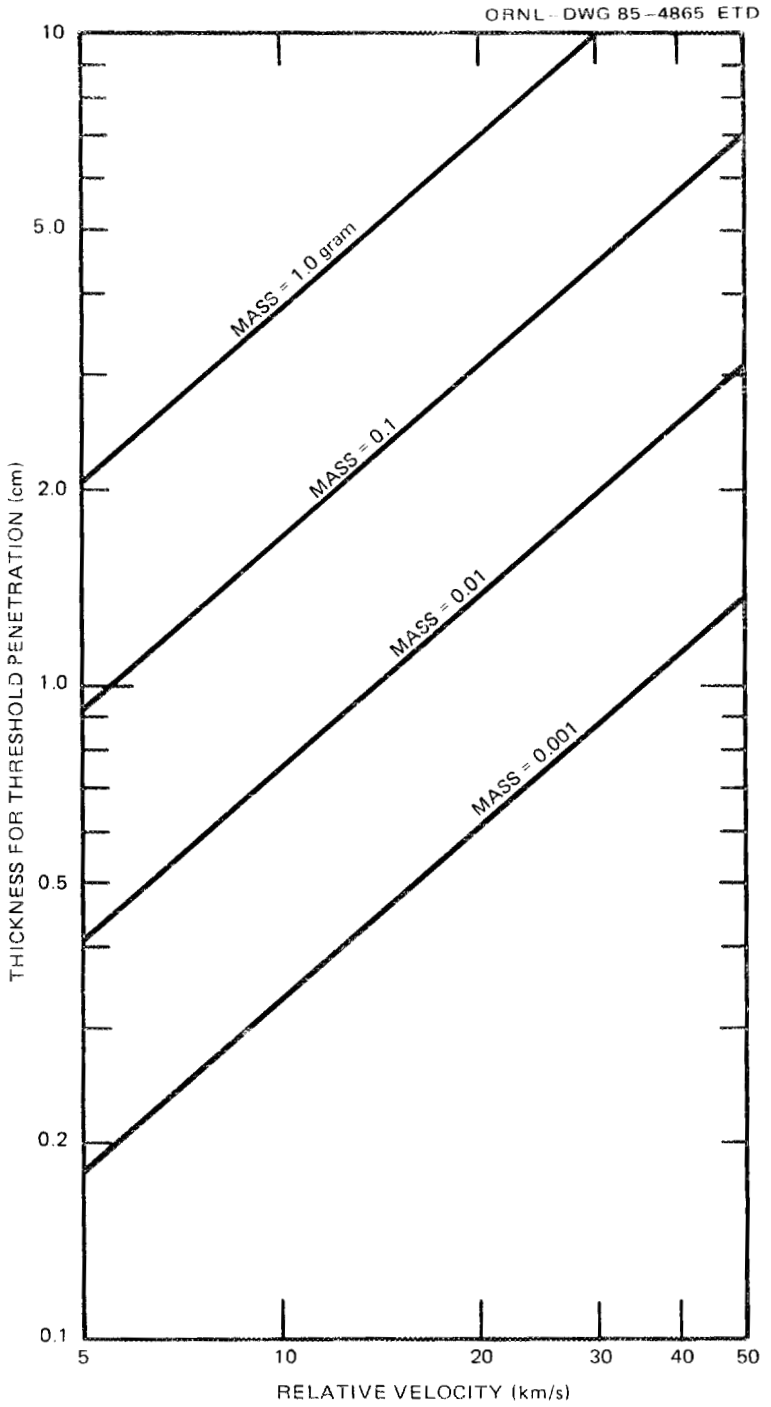

Fig. 10. Effect of relative impact velocity on thickness of aluminum 2024-T3 required for threshold penetration by meteoroids with density of 0.5 g/cm^3. (Calculated from Eq. 4.)

Table 3. Ratio of the threshold penetration thickness for various target and projectile materials to that with an aluminum target and a projectile with density of 0.5 g/cm^3

Projectile material	Target material		
	Aluminum (K_1 = 0.57)	Stainless steel (K_1 = 0.32)	Niobium (K_1 = 0.34)
Meteoroid (0.5 g/cm^3)	1.00	0.56	0.60
Plastic (1.0 g/cm^3)	1.12	0.63	0.67
Aluminum (2.77 g/cm^3)	1.33	0.75	0.79
Stainless steel (8.0 g/cm^3)	1.59	0.89	0.95
Niobium (8.58 g/cm^3)	1.61	0.90	0.96
Tungsten (19.2 g/cm^3)	1.84	1.03	1.10

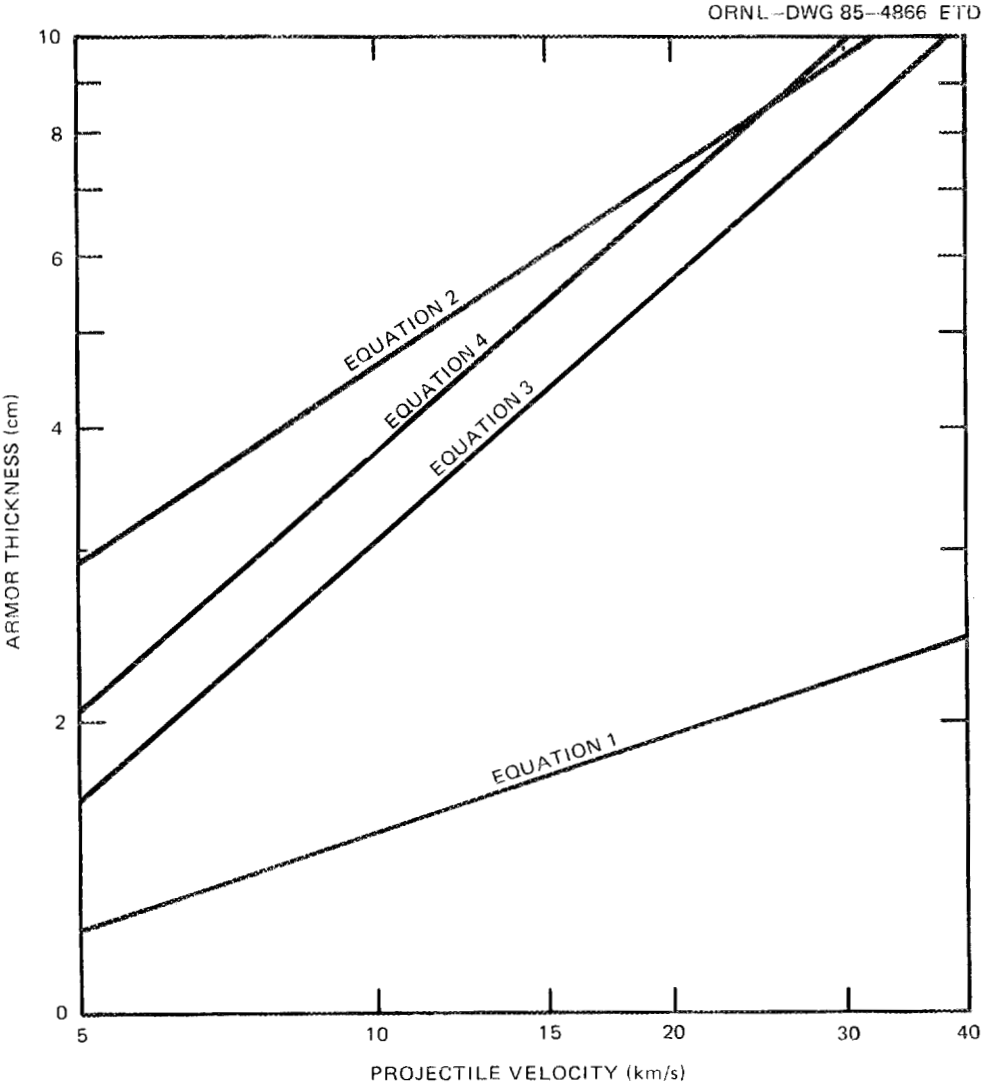

Fig. 11. Effect of projectile velocity and calculational model on estimated thickness of aluminum 2024-T3 plate required for incipient penetration by meteoroid with mass of 1 g and density of 0.5 g/cm^3.

that part of the differences between the functions is caused by the differences in the "factor of safety" applied to the penetration data to obtain the "minimum thickness" for resisting penetration. It should also be mentioned that in calculating the target thickness from Eq. 1, which is for steel, a correction was applied to obtain the thickness for aluminum. This was done by multiplying the thickness given by Eq. 1 by the ratio of the penetration constants given for different materials in Table 1 (in this case 0.57/0.32). This gives almost the same correction factor as was recommended by Bjork in 1959.

In a comprehensive parametric study conducted for NASA in 1984 by J. R. Wetch of Space Power, Inc., Eq. 4 of Ref. 8 (a 1968 NASA report) was modified to include more recent data and yielded the following expression:

$$t_s = \gamma_r a \left(\frac{\rho_p}{\rho_a}\right)^{1/2} \left(\frac{V_p}{C_a}\right)^{2/3} \left(\frac{6}{\pi \rho_p}\right)^{1/3} \left(\frac{E \alpha A_v t}{-\ln P_o}\right)^{1/3\beta} \left(\frac{2}{3n\theta\beta+2}\right)^{1/3\beta} \left(\frac{T}{T_r}\right)^{1/6} \quad (5)$$

where

t_s = armor thickness, cm;
γ_r = room temperature cratering coefficient;
a = rear surface damage thickness factor;
ρ_p = meteoroid average density, g/cm^3;
ρ_a = armor density, g/cm^3;
V_p = meteoroid average velocity, km/s;
C_a = sonic velocity in the armor, km/s;
E = armor earth shielding factor;
α = meteoroid flux constant;
A_v = vulnerable area, m^2;
t = mission time, s;
P_o = design probability of no critical damage;
n = damage factor for oblique impact;
θ = penetration constant;
β = meteoroid flux constant;
T = armor temperature, K;
T_r = room temperature, K.

As in Ref. 6, a curve similar to Fig. 1 was approximated with an empirical expression, and this empirical expression for the incidence of meteoroids as a function of their mass was combined with an empirical equation for penetration similar to Eq. (2) to yield Eq. (5). Equation (5) was then used in a computer model designed to define the weights of radiators for a wide variety of systems and conditions, and has been included here because it could prove useful for later studies. This equation is so complex that no effort to rationalize it will be made here other than to say that the rationalization can be carried out by utilizing information presented above. Further, a similar but less complex equation was developed by John C. Moyers after he reviewed a draft of this report. That equation, with its derivation, has been included in the Appendix.

4. PROTECTIVE BUMPERS

As early as 1947, Whipple pointed out that the shock wave associated with the impact of a meteoroid on even a very thin bumper would shatter the meteoroid, particularly in view of the fact that most meteoroids are a porous, stoney material and therefore are not only brittle but quite frangible. This effect would be particularly pronounced if part of the bumper were completely vaporized by the impact, so that expansion of the cloud of vapor would disperse the debris of the meteoroid. The impact of the cloud on the protected structure would not induce serious stresses or damage if it were distributed over a wide area of the underlying structure by using a relatively large separation distance. This approach was considered in design studies at both ORNL and NASA in 1959,[3] and an extensive test program was conducted by NASA. One of the more important results of this effort was the design and testing of a bumper system in a satellite in the latter 1970s. The results of this experiment showed that the type of bumper design that was tested would serve to reduce the weight of the meteoroid protection system by a factor of ~6.9 (Ref. 22).

The problems posed by the design of bumpers are more complex than those involved in preventing penetration during hypervelocity impact. Valuable insights and helpful design information are presented in Ref. 5, but the new problems posed by the high incidence of spacecraft debris raise questions not treated there. Relatively little new experimental information on laboratory tests of bumpers has emerged since publication of Ref. 5 in 1970. The bulk of solid particle impact data obtained with light gas guns extends only up to velocities of 10 km/s. Fortunately, this is in the right range for the relative velocities of the spacecraft debris that is orbiting in roughly the same direction as most spacecraft but is below the lower limit of the range for both extraterrestrial meteoroids and particles that might be launched in retrograde orbits in attacks on satellites. This is important because in the low relative velocity region much of the incident particle is not vaporized (see Fig. 9), and experiments show that particles emitted from an impact with a bumper may be large enough to damage the surface that

the bumper was designed to protect irrespective of the separation distance. On the other hand, for relative velocities of 20 km/s or more, the incident particle may be completely vaporized by the bumper, and the resulting plasma will expand rapidly so that the probability of damaging a protected surface will fall off rapidly with the separation distance between the bumper and the surface it is designed to protect. The available experimental data do not appear to be adequate to evaluate some interesting possibilities in this region. Unfortunately, it is exceedingly difficult to produce projectile velocities >12 km/s in controlled experiments. The problems are so formidable that up to the time of this writing no viable test system has been demonstrated.

The first step in analyzing the effects of a bumper is to consider the exchange of momentum and energy when the projectile strikes the bumper. Some experimental data indicate that the collision is inelastic, and that the mass of the projectile and the slug punched out of the bumper emerge from the collision at essentially the same velocity. The reduction in projectile velocity as determined from momentum considerations results in a loss of kinetic energy that is greater than the kinetic energy imparted to the slug of material punched from the bumper. This energy appears as heat. Quantitatively, this "excess energy" is given by a simple derivation as:

$$E_h = \frac{m_p}{2}\left(\frac{m_b}{m_p + m_b}\right) V^2 \qquad (6)$$

where

E_h = energy appearing at heat, J

m_p = mass of projectile, kg;

m_b = mass of slug punched from bumper, kg;

V = velocity of projectile, m/s.

While the distribution of this heat is uncertain, there are indications that roughly one-half appears in the projectile, and the remainder is in the material punched from the bumper. Assuming this to be the case, Table 4 and Fig. 12 were prepared to show the thermal energy input to both the projectile and the bumper as a function of the projectile

Table 4. Kinetic energy dissipated as thermal energy in meteoroid collisions with a bumper. This heat energy was assumed to be divided equally between the meteoroid and the slug punched from the bumper

Meteoroid mass (g)	Bumper mass (g)	Relative velocity (m/s)	Meteoroid energy (J)	$\frac{m_b}{m_p + m_b}$	Energy dissipated (J)	Energy to meteoroid (J/g)	Energy to bumper (J/g)
1.00	0.01	5,000	12,500	0.0099	123.76	62	6,188
1.00	0.01	7,000	24,500	0.0099	242.57	121	12,129
1.00	0.01	10,000	50,000	0.0099	495.05	248	24,752
1.00	0.01	15,000	112,500	0.0099	1,113.86	557	55,693
1.00	0.01	20,000	200,000	0.0099	1,980.20	990	99,010
1.00	0.02	5,000	12,500	0.0196	245.10	123	6,127
1.00	0.02	7,000	24,500	0.0196	480.39	240	12,010
1.00	0.02	10,000	50,000	0.0196	980.39	490	24,510
1.00	0.02	15,000	112,500	0.0196	2,205.88	1,103	55,147
1.00	0.02	20,000	200,000	0.0196	3,921.57	1,961	98,039
1.00	0.05	5,000	12,500	0.0476	595.24	298	5,952
1.00	0.05	7,000	24,500	0.0476	1,166.67	583	11,667
1.00	0.05	10,000	50,000	0.0476	2,380.95	1,190	23,810
1.00	0.05	15,000	112,500	0.0476	5,357.14	2,679	53,571
1.00	0.05	20,000	200,000	0.0476	9,523.81	4,762	95,238
1.00	0.1	5,000	12,500	0.0909	1,136.36	568	5,682
1.00	0.1	7,000	24,500	0.0909	2,227.27	1,114	11,136
1.00	0.1	10,000	50,000	0.0909	4,545.45	2,273	22,727
1.00	0.1	15,000	112,500	0.0909	10,227.27	5,114	51,136
1.00	0.1	20,000	200,000	0.0909	18,181.82	9,091	90.909

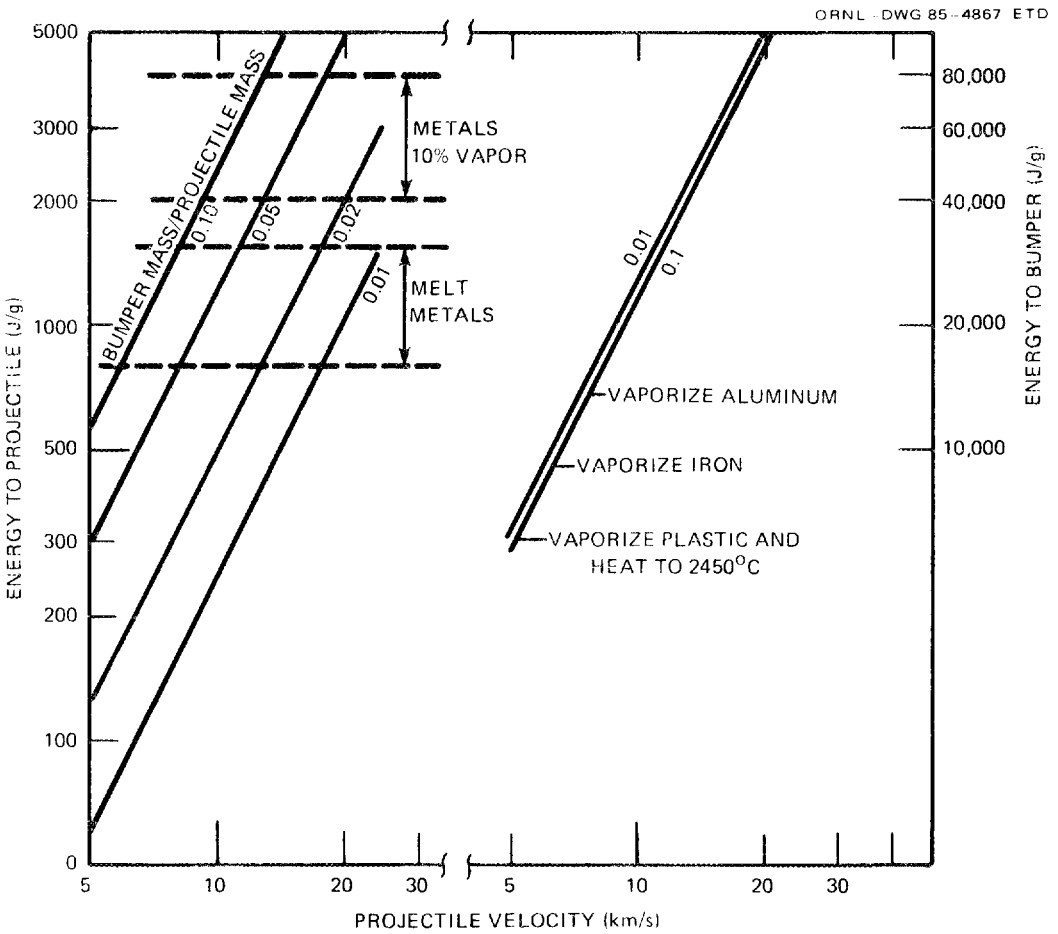

Fig. 12. Effect of impact velocity on residual energy appearing as heat in projectile and debris from the bumper assuming an inelastic collision and an equal division of the heat between the two.

incident velocity for ratios of ejected bumper mass to projectile mass ranging from 0.01 to 0.10. The notation on Fig. 12 indicates the regions where melting or vaporization might occur. While there is no notation on the curves for SiO_2, BeO, Al_2O_3, MgO, and SiC, it happens that their specific heats are such that the scale in joules per gram is about the same as that for their temperature rise in degrees Celsius up the point where vaporization or decomposition occurs, that is, in the range of 1800 to 2100°C.

Other data that are useful in evaluating the performance potential of bumpers are presented in Table 5 and Fig. 13. Figure 13 shows the temperature of typical metals as a function of the heat input up to the point of complete vaporization. These curves reveal why Fig. 12 indicates that the projectile velocity required to vaporize an iron bumper is lower than for an aluminum bumper for the same mass of metal per unit area of bumper. Note that the most easily vaporized metals listed in Table 5 are lead, bismuth, tin, silver, platinum, and gold, which implies that one of these metals should be considered for use in bumpers, and that alloys (such as solder alloys) can be developed that have significantly better characteristics for bumpers than pure metals. If a bumper is used to protect the manifolds for a radiator, the material chosen should have both a fairly high melting point and not too high a vapor pressure (to avoid excessive loss of material into the high vacuum of space).

Some pertinent results from light gas gun experiments (Ref. 5) are presented in Fig. 14. These curves show that if a bumper is employed, the penetration of the second plate is insensitive to the projectile velocity for velocities between 5 and 10 km/s. Accompanying data indicate that there is no incentive to employ a separation distance between the bumper and the protected surface greater than 20 times the diameter of the projectile. However, both of these observations appear to the writer to be applicable only to the velocity range covered in the experiments. The rationale for this view is that when the bumper is penetrated at relatively low hypervelocities, the diameter of the affected region in the bumper is possibly double the projectile diameter. Note that the diagrams of Fig. 6 show severe distortion of the

Table 5. Physical properties of some typical metals that might by used as armor or bumpers for spacecraft

Metal	Atomic weight	Melting point (°C)	Boiling point (°C)	Heat of fusion (kcal/g mol)	Heat of vaporization (kcal/g mol)	c_p 0°C to mp (cal/g mol)	c_p mp to bp (cal/g mol)
Magnesium	24.3	650	1090	2.14	31.5	6.80	8.02
Lithium	6.9	179	1317	1.10	32.5	6.9	6.9
Beryllium	9.01	1278	2970	2.34	68.0	4.05	7.01
Aluminum	27	660	2467	2.57	67.9	5.84	6.94
Titanium	47.9	1675	3260	4.50	102.5	7.3	8.9
Chromium	52	1890	2482	3.50	73.0	8.8	11.6
Cadmium	112.4	321	765	1.48	32.2	7.1	7.1
Iron	55.8	1535	3000	3.30	84.6	7.7	11.1
Cobalt	58.9	1492	2900	3.70	93.0	10.1	9.7
Nickel	58.7	1453	2732	4.21	89.6	7.47	10.1
Copper	63.5	1083	2595	3.12	72.8	6.16	7.5
Zinc	65.4	420	906	1.60	27.4	7.81	7.01
Niobium	93	2468	4927	6.40	166.5	7.1	7.7
Molybdenum	96	2610	5560	6.60	142.0	9.1	8.5
Silver	108	961	2212	2.65	61.6	6.5	7.4
Tungsten	184	3410	5927	8.42	197.0	7.1	7.4
Tin	118.7	232	2270	1.72	68.0	6.9	9
Rhenium	186	3180	5627	8.00	178.0	7.8	8.2
Platinum	195	1769	3827	4.70	112.1	6.96	8.4
Gold	197	1063	2966	3.05	82.0	6.28	7.1
Bismuth	209	271	1477	2.51	42.6	7.1	8.7
Lead	207	327	1737	1.22	42.4	8.1	7.7

Metal	Enthalpy (J/g) above 0°C				Sound velocity (m/s)
	To melting point	To liquid	To boiling point	To gas	
Magnesium	762	1,131	1,739	7,166	5,910
Lithium	749	1,417	6,182	25,903	
Beryllium	2,405	3,493	9,005	40,605	12,890
Aluminum	598	996	2,941	13,471	6,890
Titanium	1,069	1,462	2,695	11,655	6,560
Chromium	1,339	1,621	2,174	8,052	
Cadmium	85	140	257	1,457	
Iron	887	1,135	2,355	8,703	6,400
Cobalt	1,071	1,334	2,305	8,916	6,220
Nickel	774	1,074	1,996	8,387	5,910
Copper	440	641	1,393	6,194	5,250
Zinc	210	312	531	2,285	
Niobium	789	1,077	1,929	9,426	2,580
Molybdenum	1,036	1,324	2,417	8,611	6,250
Silver	242	345	704	3,092	3,940
Tungsten	551	743	1,166	5,649	5,750
Tin	56	117	764	3,163	
Rhenium	558	738	1,190	5,197	
Platinum	264	365	736	3,143	2,950
Gold	142	207	494	2,237	2,950
Bismuth	39	89	299	1,152	1,800
Lead	54	78	298	1,155	1,250

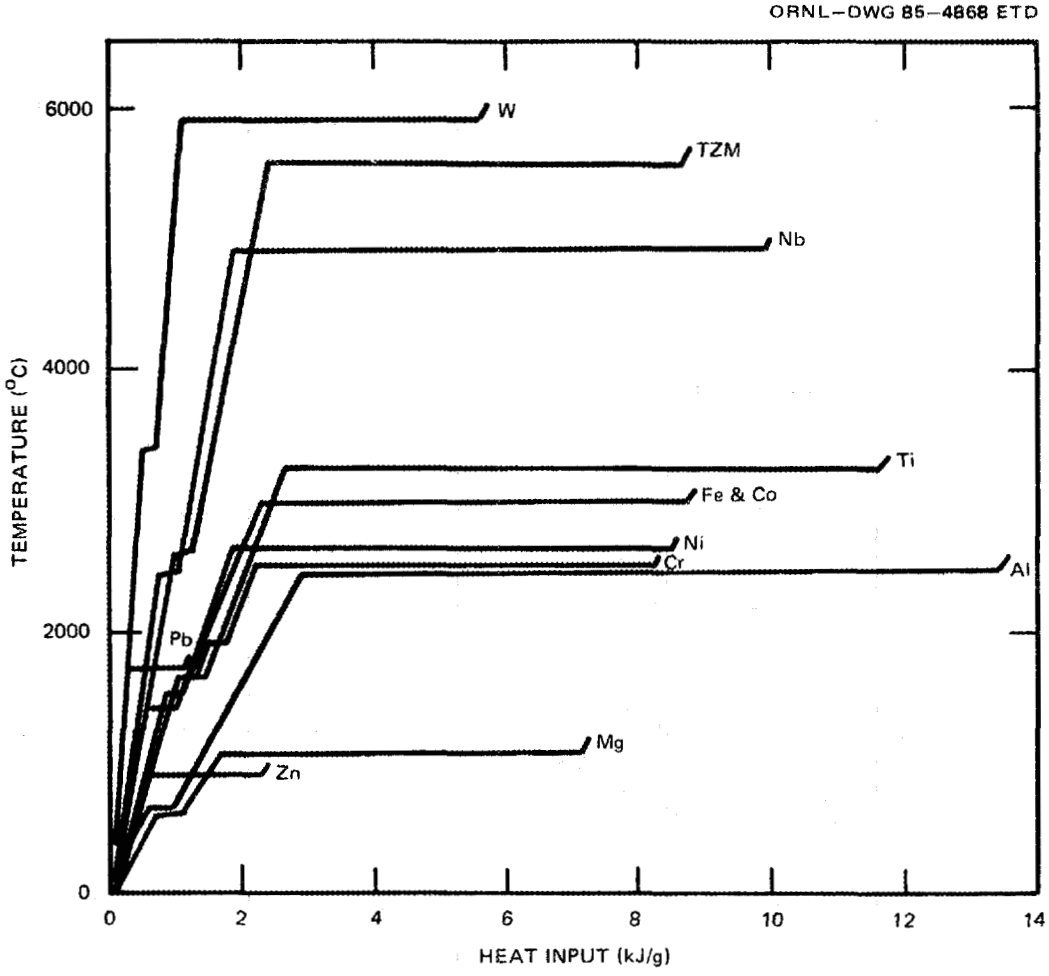

Fig. 13 (a). Temperature rise above 0°C as function of heat input for typical metals. Data plotted from Table 5.

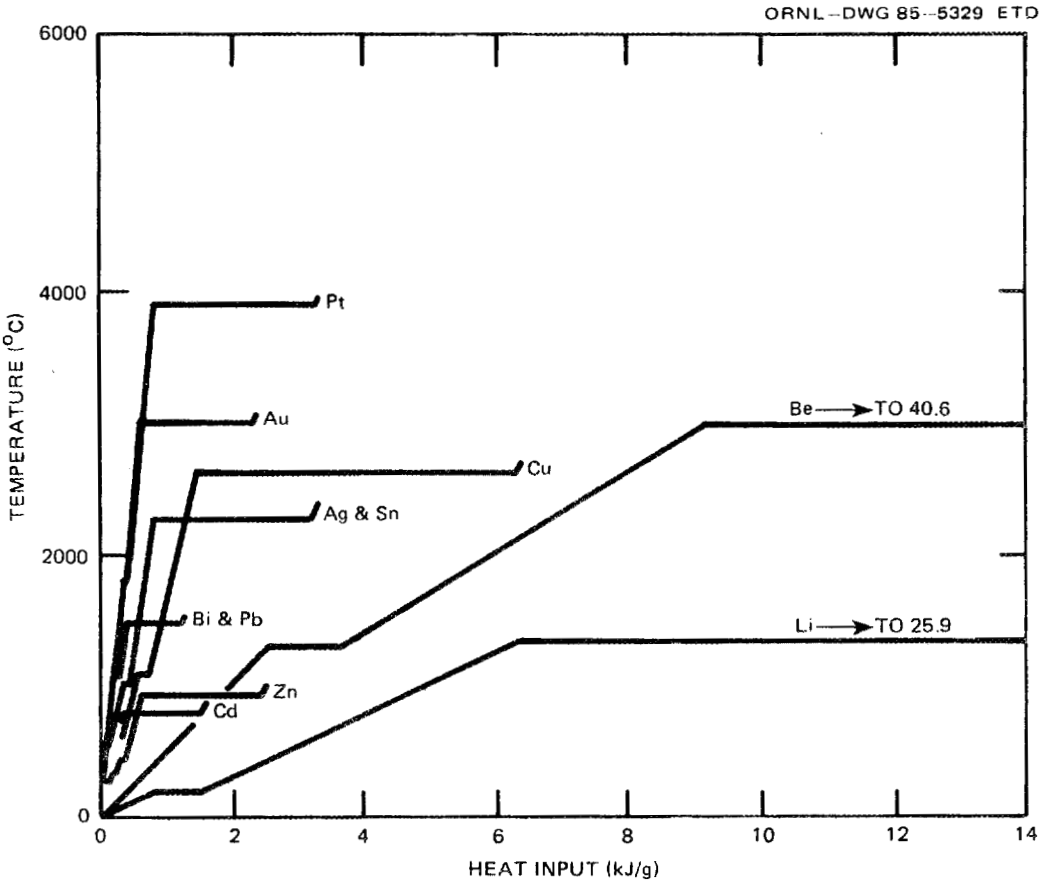

Fig. 13 (b). Temperature rise above 0°C as function of heat input for typical metals. Data plotted from Table 5.

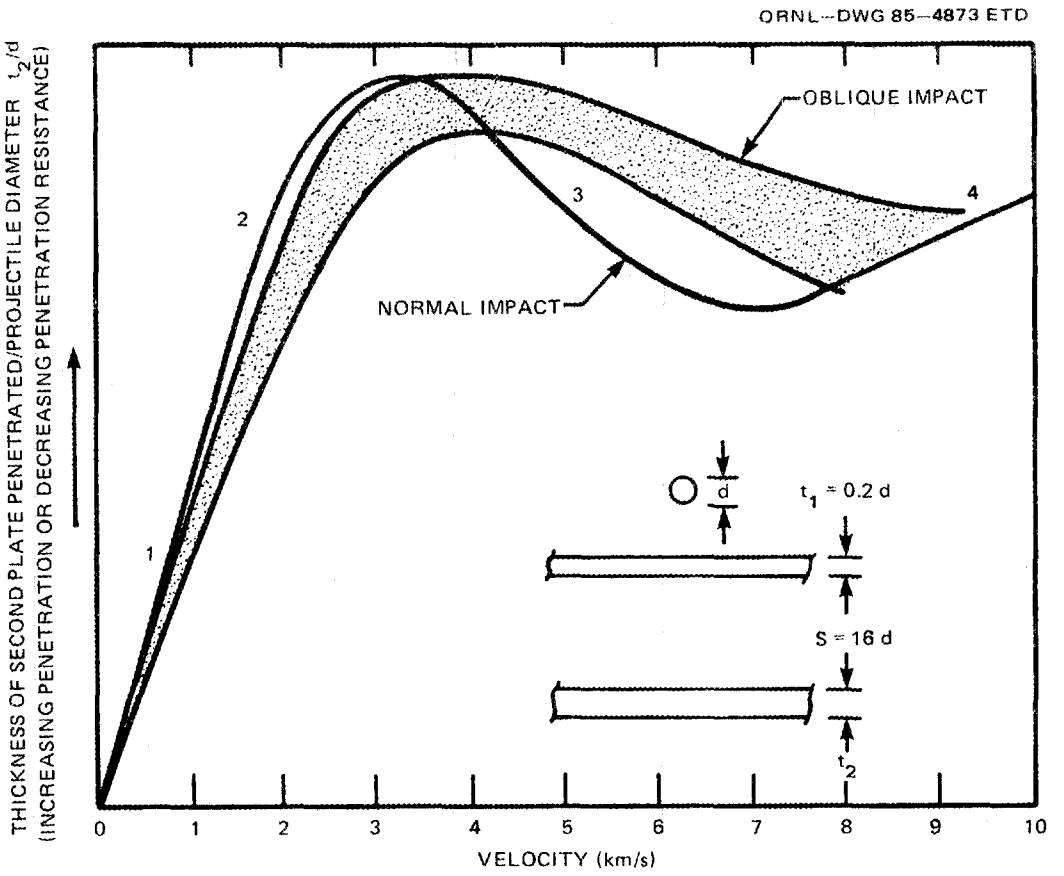

NOTES:

NUMBERS ON NORMAL IMPACT CURVE SHOW THE VARIATION OF DEBRIS WITH VELOCITY

1. INTACT PROJECTILE
2. TIGHT CLUSTER OF RELATIVELY LARGE FRAGMENTS OF PROJECTILE AND SHIELD
3. DEBRIS IN SHAPE OF ELONGATED BUBBLE WITH SURFACE COMPOSED OF NUMEROUS SMALL SOLID PARTICLES OF PROJECTILE AND SHIELD
4. DEBRIS CONSISTING OF:
   A. ELONGATED BUBBLE COMPOSED OF VERY SMALL SOLID PARTICLES, MINUTE DROPS OF MELTED METAL, AND METAL VAPOR
   B. A FEW SOLID FRAGMENTS WHICH ARE LARGER AND SLOWER THAN THE BALANCE OF DEBRIS

Fig. 14. Schematic description showing both the penetration resistance of a target and the character of the debris vary as a function of the velocity for aluminum projectiles and aluminum alloy bumpers and targets. Source: *Meteoroid Damage Assessment*, NASA SP-8042, National Aeronautics and Space Administration, May 1970.

bumper in this region during impact. Relatively large fragments are torn off the bumper from outside the nominal edge of the hole, and these become a major source of potential damage to the underlying surface. This is especially the case if the velocity of the fragments is sufficiently below that of the projectile so that it falls in the high subsonic region where the depth of penetration can be greater than in the hypersonic region.

For very high projectile velocities such as those projected for the vicinity of the Halley's Comet encounter (e.g., 57 km/s), both the projectile and the bumper should be vaporized irrespective of the materials involved. An interesting treatment of this region is presented in Ref. 23, but some of the conclusions drawn apply only to the special case treated, that is, to a pair of infinite plates. These conclusions probably are not applicable to the more complex geometry of concentric cylindrical shells in which the bumper shell diameter may be several times that of the radiator vapor manifold it is designed to protect.

Useful design data for single or dual element shields to protect against very high velocity (57 km/s) impacts by typical comet fragments are given in Ref. 21 for an assumed particle density of 0.8 g/cm^3. This study was carried out by the Ballistics Research Laboratory at the Aberdeen Proving Ground of the U.S. Army; hence the approach and nomenclature used are somewhat different from the usual practice in the space community. In particular, they define two cases (i.e., one-element and two-element shields) and analytically evaluate conditions that would lead to incipient penetration in each case. Thus, these two cases correspond to the cases considered above, with or without a bumper. The geometrical arrangement and nomenclature used for analysis of the systems with single and dual shields are shown in Figs. 15 and 16. The spacing between the two elements was taken as approximately twenty times the diameter of the incident particle. Figure 17 shows estimated masses of comet fragments for incipient penetration of the single element shields. Figure 18 shows the effectiveness of a bumper. In this case a 1-mm-thick bumper, or first shield element, protects the base surface, or second shield element sufficiently to prevent its penetration by

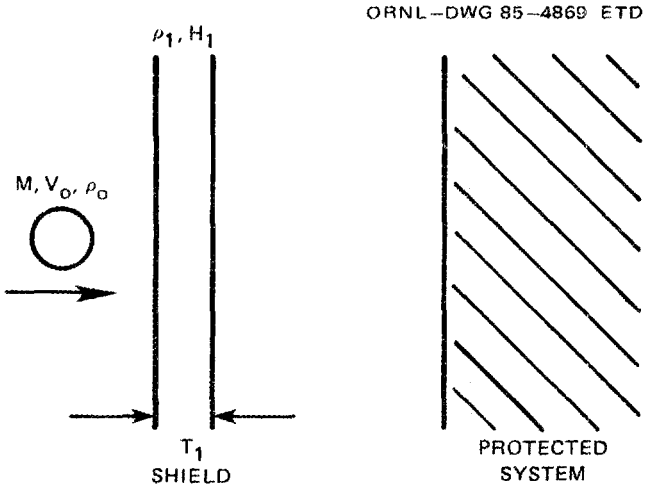

Fig. 15. Geometrical arrangement and nomenclature for analysis of single impact shield. Source: J. H. Kineke, Jr., "Probe Protection Against Cometary Meteoroid Attack," pp. 77–83 in *Proceedings of The Comet Halley Micrometeoroid Hazard Workshop*, Noordwijk, Netherlands, 18–19 April, 1979, European Space Agency, ESA-SP-153.

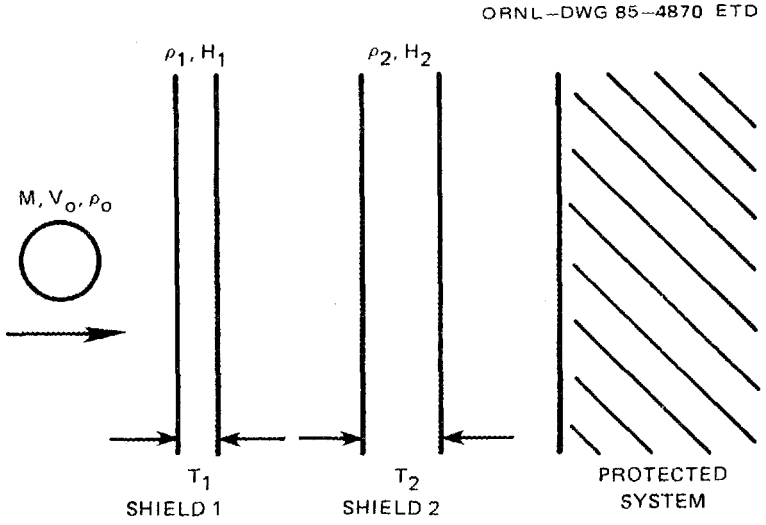

Fig. 16. Geometrical arrangement and nomenclature for analysis of a dual impact shield. The spacing between the two elements of the shield was taken as approximately 20 times the diameter of the projectile. Source: J. H. Kineke, Jr., "Probe Protection Against Cometary Meteoroid Attack," pp. 77–83 in *Proceedings of The Comet Halley Micrometeoroid Hazard Workshop*, Noordwijk, Netherlands, 18–19 April, 1979, European Space Agency, ESA-SP-153.

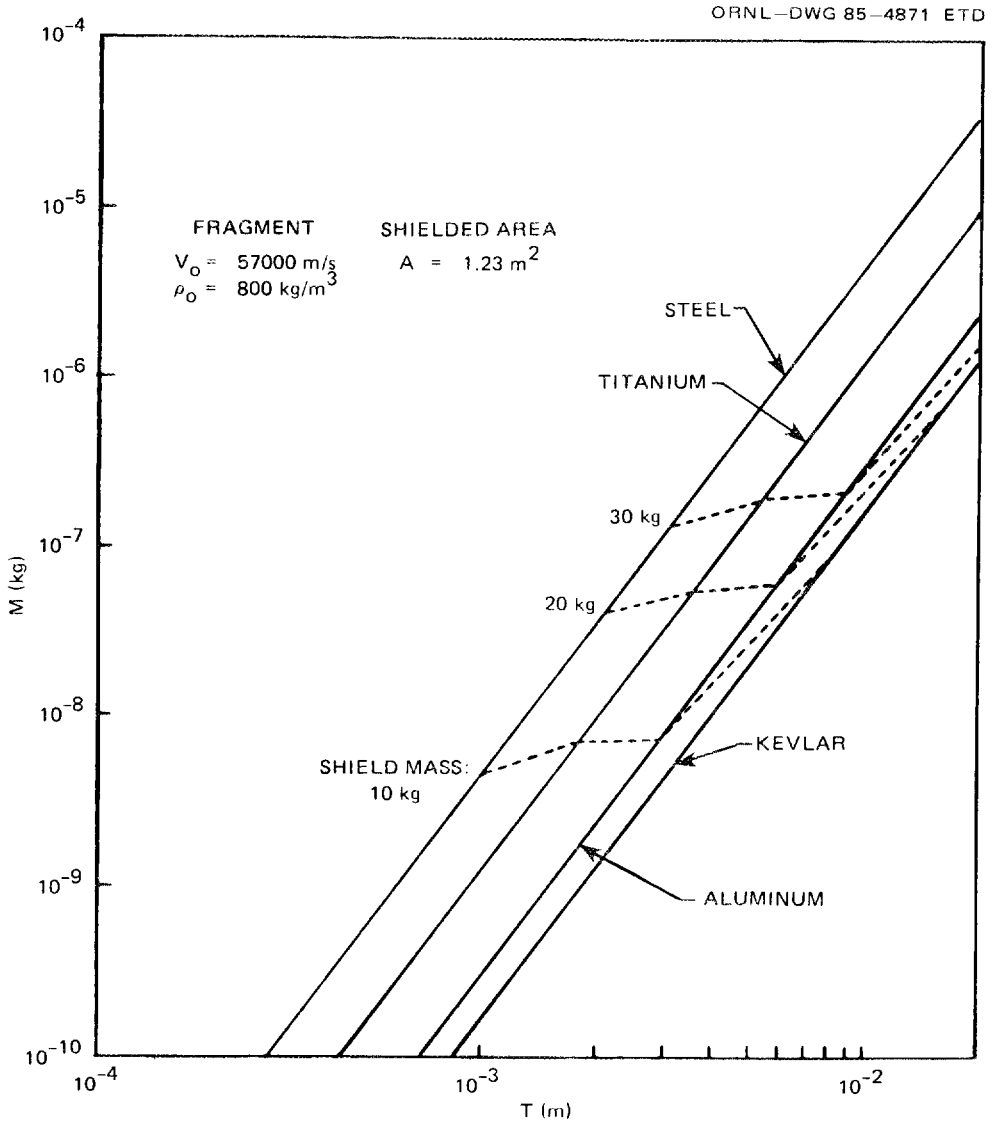

Fig. 17. Estimated mass M of comet fragment required for incipient penetration of various monolithic shield materials as function of shield thickness T for a single element shield. Source: J. H. Kineke, Jr., "Probe Protection Against Cometary Meteoroid Attack," pp. 77–83 in *Proceedings of The Comet Halley Micrometeoroid Hazard Workshop*, Noordwijk, Netherlands, 18–19 April, 1979, European Space Agency, ESA-SP-153.

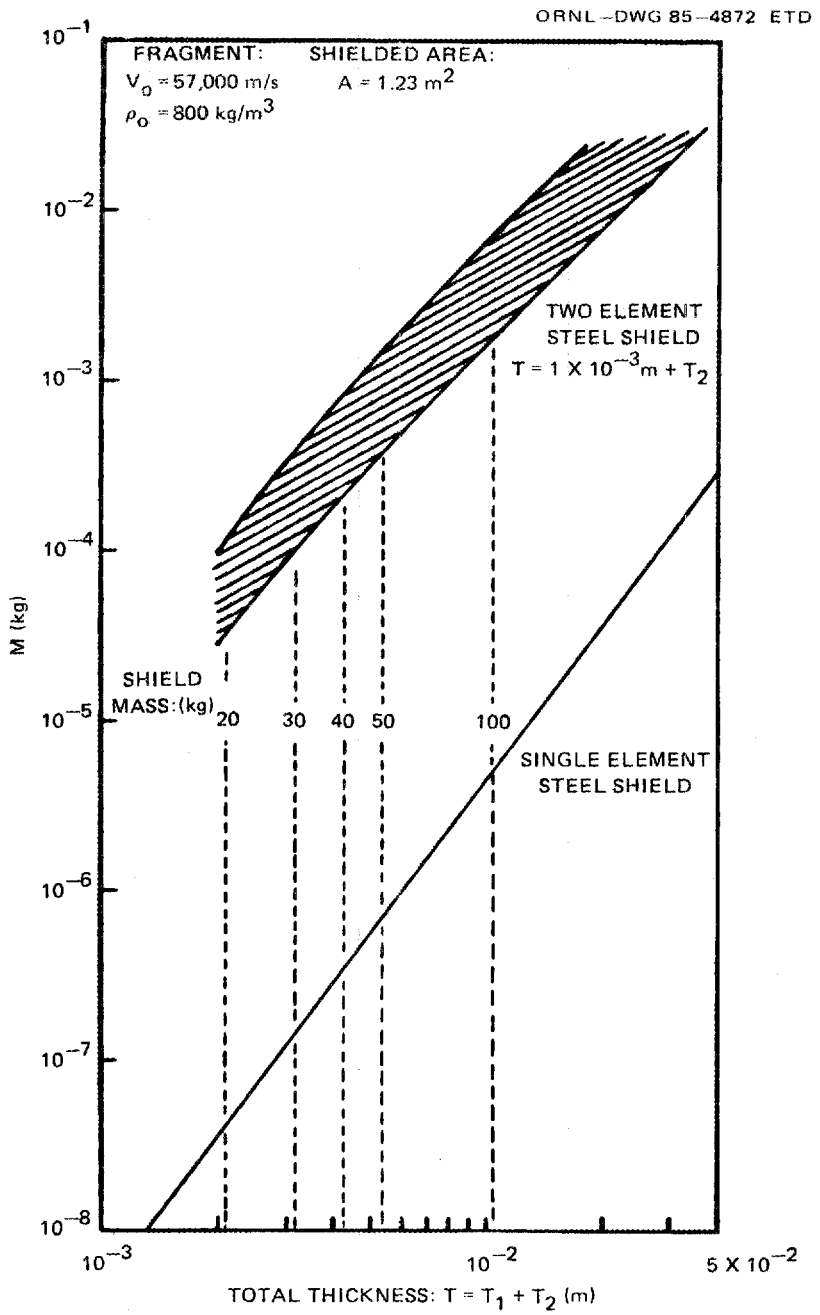

Fig. 18. Estimated mass M of comet fragment required for threshold penetration of single element and two element steel shields as function of total thickness of shield(s). Source: J. H. Kineke, Jr., "Probe Protection Against Cometary Meteoroid Attack," pp. 77–83 in *Proceedings of The Comet Halley Micrometeoroid Hazard Workshop*, Noordwijk, Netherlands, 18–19 April, 1979, European Space Agency, ESA-SP-153.

fragments up to 1000 times heavier than those that would penetrate the same total thickness in the form of a single shield.

Figures 19–21, also reproduced from Ref. 21, show results of calculations of the effect of impacts of comet fragments on two-element shields in which the first shield element (bumper) consists of 1.0 mm of steel, titanium, and aluminum, respectively. In each case curves are provided for four different materials for the second, or base, armor plate. These four materials for each set of curves are 440C stainless steel, titanium, aluminum, and Kevlar (this is the epoxy-impregnated, multilayered cloth composite used in armored vests). Note that aluminum gives somewhat lighter shields than the other two metals, but that Kevlar shields are much lighter than the aluminum. Unfortunately, the Kevlar would not be suitable for the protection of a red-hot radiator for a nuclear electric space power plant.

The use of a plastic, or composite, bumper seems promising because the plastic will vaporize at much lower impact velocities than any metal. However, it may not be suitable for use with high-temperature radiators. If a large clear plastic bubble were inflated around the radiator, its equilibrium temperature would depend upon its transmittance in the infrared region together with its emissivity. The limited data available for clear plastics make this approach doubtful for the high-temperature radiators now being considered because the plastic bubble would have to be unreasonably large to maintain its temperature at a suitable level, making the bumper weight excessive. This concept should be examined further, however, in the hope of finding a plastic material with sufficiently favorable properties.

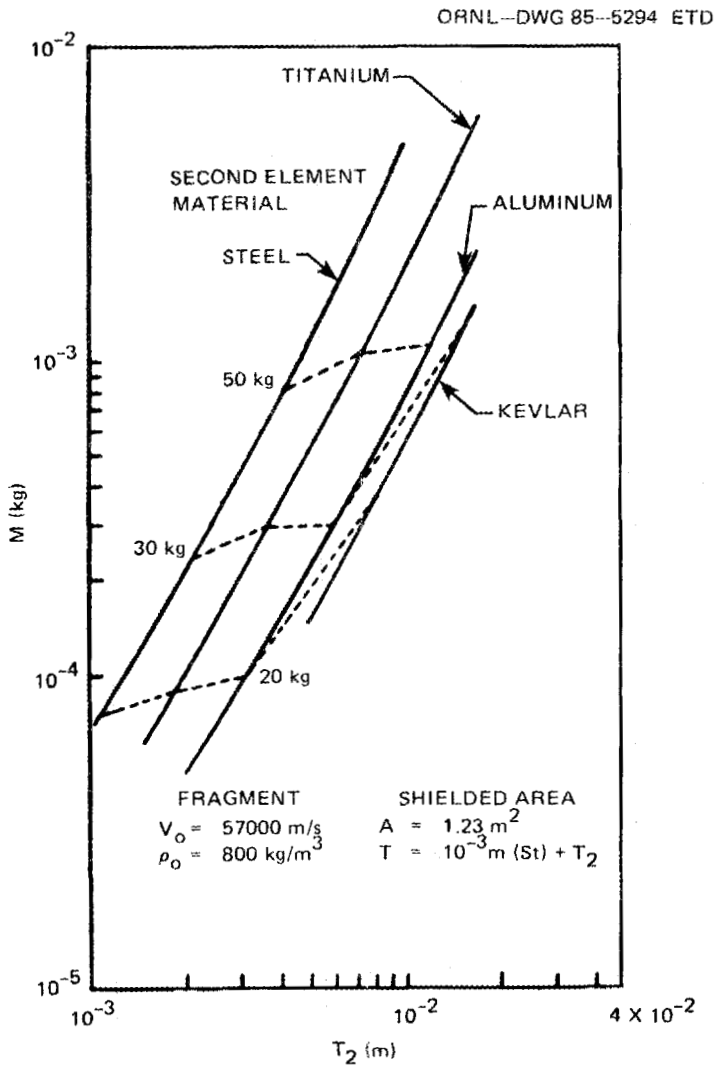

Fig. 19. Estimated mass M of comet fragment required for threshold penetration of various shield materials as function of shield thickness T_2 for operation with a 1.0-mm-thick bumper of stainless steel. Source: J. H. Kineke, Jr., "Probe Protection Against Cometary Meteoroid Attack," pp. 77–83 in *Proceedings of The Comet Halley Micrometeoroid Hazard Workshop*, Noordwijk, Netherlands, 18–19 April, 1979, European Space Agency, ESA-SP-153.

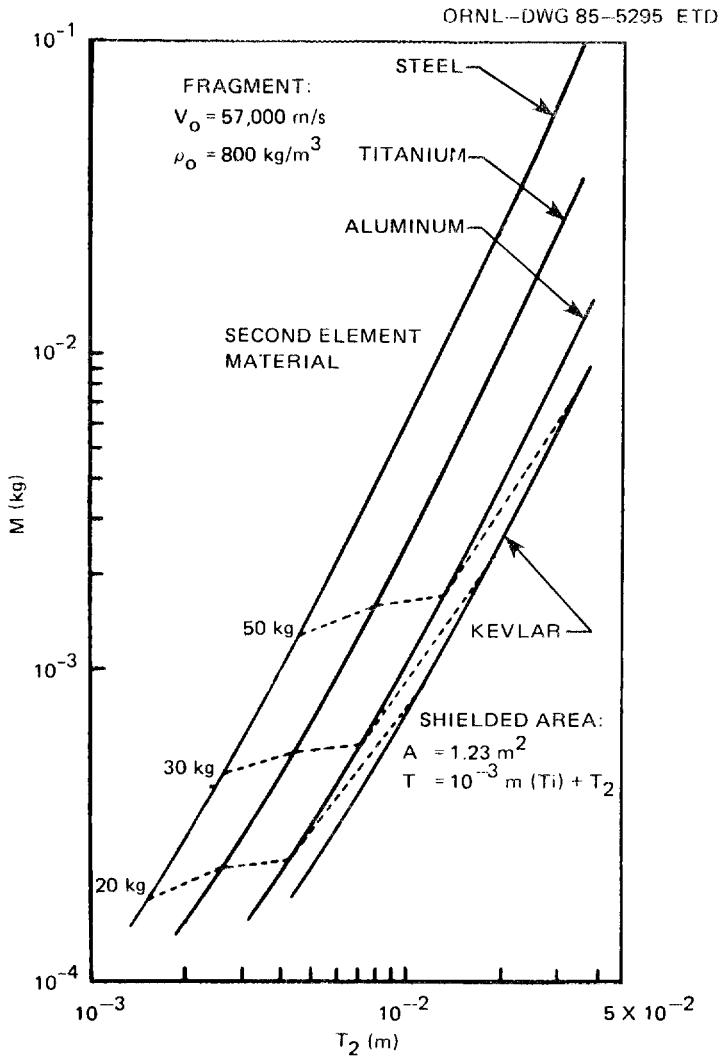

Fig. 20. Estimated mass M of comet fragment required for threshold penetration of various shield materials as function of shield thickness T_2 for operation with a 1.0-mm-thick bumper of titanium. Source: J. H. Kineke, Jr., "Probe Protection Against Cometary Meteoroid Attack," pp. 77–83 in *Proceedings of The Comet Halley Micrometeoroid Hazard Workshop*, Noordwijk, Netherlands, 18–19 April, 1979, European Space Agency, ESA-SP-153.

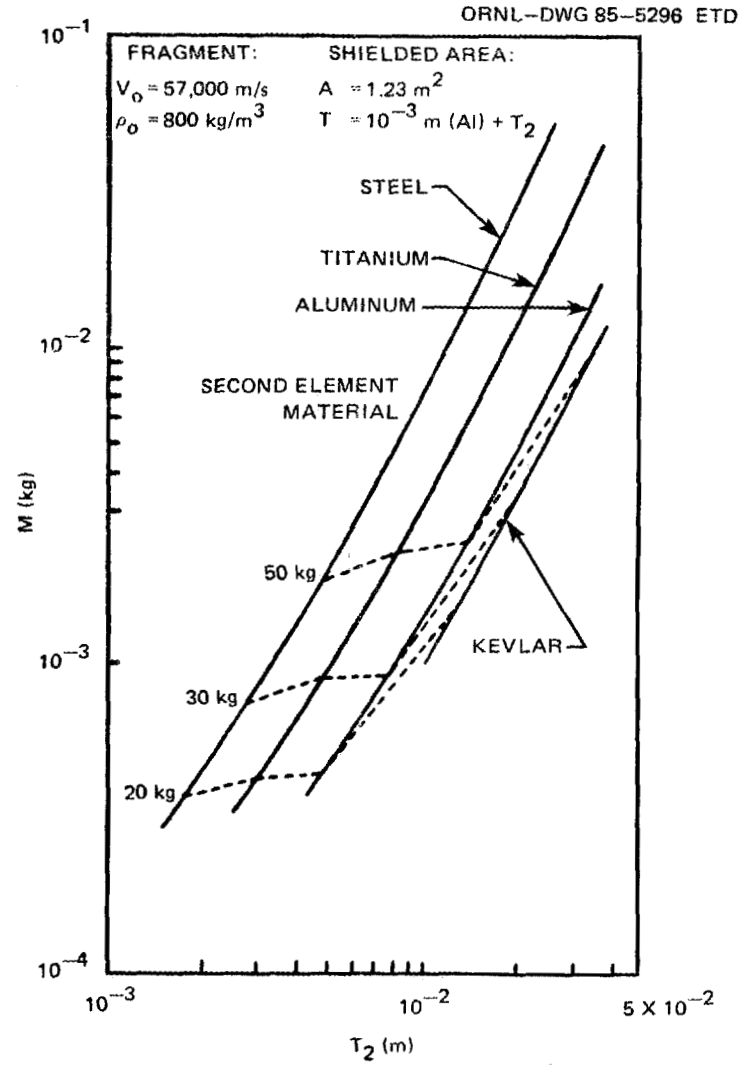

Fig. 21. Estimated mass M of comet fragment required for threshold penetration of various shield materials as function of shield thickness T_2 for operation with a 1.0-mm-thick bumper of aluminum. Source: J. H. Kineke, Jr., "Probe Protection Against Cometary Meteoroid Attack," pp. 77–83 in *Proceedings of The Comet Halley Micrometeoroid Hazard Workshop*, Noordwijk, Netherlands, 18–19 April, 1979, European Space Agency, ESA-SP-153.

5. CONCLUSION

Sufficient information is available for the preliminary analysis of conceptual impact shield designs. Further experimental results are badly needed, however, to permit a thorough job of evaluating the effectiveness of bumpers for protection against solid particle impacts in the velocity range from 10 to 30 km/s. It is particularly important to obtain data on the effects of both bumper and projectile material on the size of fragments produced, their velocities, and the cone angles of the shower of fragments and/or gas produced during the solid particle impact on the bumper. Although the velocity of sound in steel runs approximately 6 km/s (see Table 5), the velocity of sound in plastics runs 2 to 3 km/s. This should be sufficient to vaporize the slug punched from a plastic bumper. Impact studies of plastic and/or composite bumpers at low hypersonic velocities would greatly increase the flexibility of shield design. Experiments should be performed to investigate the use of surface coatings on the bumper to maintain bumper temperatures within thermal limits of the plastic and/or composite materials.

REFERENCES

1. F. L. Whipple, *The Meteoritic Risk to Space Vehicles, Vistas in Aeronautics*, Pergamon Press, New York, 1968, pp. 115–24.

2. G. M. Anderson and A. P. Fraas, Conference on the Meteoroid Hazard to Space Power Plants, Dec. 1 and 2, 1959, Washington, D.C.

3. R. J. Hefner and P. G. Lafyatis, *Protection of Space Vehicles from Meteorite Penetration*, ORNL/CF 60-1-67, Union Carbide Corp. Nuclear Div., Oak Ridge Natl. Lab., Jan. 20, 1960.

4. B. G. Cour-Palais, *Meteoroid Environment Model — 1969 (Near Earth to Lunar Surface)*, NASA Space Vehicle Design Criteria (Environment), NASA SP-8013, National Aeronautics and Space Administration, 1969.

5. *Meteoroid Damage Assessment*, NASA SP-8042, National Aeronautics and Space Administration, May 1970.

6. H. C. Haller and S. Lieblein, *Analytical Comparison of Rankine Cycle Space Radiators Constructed of Central, Double, and Block-Vapor-Chamber Fin-Tube Geometries*, NASA Technical Note TN D-4411, National Aeronautics and Space Administration, February 1968.

7. G. L. Yoder, *Parametric Study of the Weight of Space Radiators*, Oak Ridge Natl. Lab. study carried out for NASA under agreement NOEW/1983-14, July 1984 (unpublished).

8. J. R. Wetch, *Megawatt Class Nuclear Space Power Systems*, Space Power Inc., Report No. SP-57-5-84, prepared for NASA Lewis Research Center under Contract No. NAS 3-23867, November 1984.

9. D. J. Kessler and B. G. Cour-Palais, "Collision Frequency of Artificial Satellites: The Creation of a Debris Belt", *J. Geophys. Res.* 83 (A6), 2637–46 (June 1, 1978).

10. B. G. Cour-Palais, *Space Vehicle Shielding Design*, ESA SP-153, European Space Agency, 1979.

11. B. R. Sperber, "Orbital Debris Avoidance in Low Earth Orbit," Paper presented at the AIAA 19th Aerospace Sciences Meeting, Jan. 12–15, 1981, St. Louis, Mo.

12. *Orbital Debris*, Proceedings of a Workshop Held at NASA Lyndon B. Johnson Space Center, Houston, Tex., July 27–29, 1982.

13. L.G. Taff et al., "Low Altitude, One Centimeter, Space Debris Search at Lincoln Laboratory (M.I.T.) Experimental Test System," *Advances in Space Research — 1984*, Vol. 5, No. 2, pp. 35–46, Pergamon Press, New York, 1985.

14. R. Kinslow, *High Velocity Impact Phenomena*, Academic Press, New York, 1970.

15. *Proceedings of the 6th Symposium on Hypervelocity Impact*, Cleveland, Ohio, April 30—May 2, 1963, CONF-192.

16. *Proceedings of the 7th Symposium on Hypervelocity Impact*, Tampa, Fla., 1964.

17. *Proceedings of the AIAA Hypervelocity Impact Conference*, Cincinnati, Ohio, April 30—May 2, 1969

18. R. J. Eichelberger and J. H. Kineke, Jr., *Hypervelocity Impact, Kurzzeitphysik*, ed. Vollrath and Thomer, Springer-Verlag, 1967.

19. M. H. Wagner and K. H. Kreyenhagen, "Review of the Hydro-Elastic-Plastic Code Analyses as Related to the Hypervelocity Particle Impact Hazard," pp. 115—20 in *Proceedings of The Comet Halley Micrometeoroid Hazard Workshop*, Noordwijk, Netherlands, 18—19 April, 1979, European Space Agency, ESA-SP-153.

20. R. L. Bjork, personal communication to A. P. Fraas, Oak Ridge National Laboratory, December 1959.

21. J. H. Kineke, Jr., "Probe Protection Against Cometary Meteoroid Attack," pp. 77—83 in *Proceedings of The Comet Halley Micrometeoroid Hazard Workshop*, Noordwijk, Netherlands, 18—19 April, 1979, European Space Agency, ESA-SP-153.

22. D. H. Humes, *Meteoroid Bumper Experiment on Explorer 46*, NASA Technical Paper 1879, National Aeronautics and Space Administration, July 1981.

23. R. Madden, *Ballistic Limit of Double-Walled Meteoroid Bumper Systems*, NASA Technical Note TN D-3916, National Aeronautics and Space Administration, April 1967.

APPENDIX

Appendix

ESTIMATION OF THE PROBABILITY OF PERFORATION BY METEOROID IMPACT DURING MISSION LIFETIME

John C. Moyers

1. INTRODUCTION

During its useful lifetime, a vehicle in earth orbit probably will be impacted by many meteoroids. The number of impacts depends upon the particle flux, the exposed vehicle area, and the duration of the vehicle mission. The likelihood of perforation of a vital component by any one of these impacts depends upon the mass, velocity, and density of the impacting particle and the thickness and physical properties of the target material. The probability of the vehicle's suffering crippling damage from meteoroid perforation is then a function of all these factors. The following methodology permits the estimation of this probability, utilizing available information.

2. BASIC INFORMATION

The near-Earth average meteoroid flux (number of particles, of mass equal to or greater than m grams, per square meter-second) can be estimated from the model developed by Cour-Palais:[4]

$$\log_{10} N_t = -14.37 - 1.213 \log_{10} m \ . \qquad \text{(Eq. A1)}$$

This flux may be corrected for the effects of defocusing by the Earth's gravitational field and shielding by the Earth by applying the following multiplicative factors to N_t obtained from the above model. The defocusing factor, G_e, was presented by Fig. 2 in the body of the report and may be represented by the expression

$$G_e = 0.568 + 0.432/R \ ,$$

where

R = orbit radius in units of Earth radii
= $(6378 + H)/6378$ where H is orbital altitude, km.

The Earth shielding factor E is determined from the relationship

$$E = (1 + \cos \theta)/2 \ ,$$

where θ is half the angle subtended by the Earth as viewed from orbit, or

$$\theta = \arcsin [6378/(6378 + H)] \ .$$

The probability of any given particle having a given velocity was presented in Fig. 3 in the body of the report for 3 km/s intervals. It is assumed that this velocity distribution is independent of particle mass. Values for the probability of each velocity interval and the cumulative probability for velocity being equal to or greater than the velocity interval are tabulated in Table A1.

The thickness of a given material for incipient penetration by an impacting particle is estimated by Eq. 4 from the body of the report:

$$t = K_1 \, m_p^{0.352} \, \rho_p^{0.167} \, V^{0.875} \ , \qquad \text{(Eq. A2)}$$

where

t = thickness, cm,
K_1 = constant determined from Table 1 in body of report for material of interest,
m_p = mass of particle, g,
ρ_p = density of particle, g/cm^3,
V = particle velocity, km/s.

3. METHODOLOGY

The relationship for thickness for incipient penetration given in Eq. A2 may be transposed, to provide the mass (m_l) of a particle having the capability of penetrating a wall of given thickness when impacting at a given velocity, as follows.

$$m_l = t^{2.84}/(K_l^{2.84}\ \rho_p^{0.474}\ V^{2.485})\ .$$

This definition of m_l may then be substituted for m in Eq. A1 to yield an expression for the flux, N_{ti}, of particles having mass equal to or greater than the lethal mass for the given velocity, V_i. (This does <u>not</u> mean that all particles represented by this flux value are at or above the given velocity.) The resulting expression, including the correction for the Earth's shielding and gravitational field, is

$$N_{ti} = 4.266 \times 10^{-15}\ G_e\ E\ t^{-3.445}\ K_l^{3.445}\ \rho_p^{0.575}\ V_i^{3.014}\ .$$

Values of N_t are calculated from this expression for all of the 22 velocity intervals taken from Table A1.

A net flux increment is then calculated for each velocity interval and multiplied by the probability that the velocity of a given particle will be equal to or greater than the interval midpoint velocity. This product is the lethal flux increment, N_{li}, associated with the velocity interval V_i. For the lowest velocity interval, the net flux increment is equal to N_{t1} as determined from the above expression, representing all particles having mass equal to or greater than the lethal mass for this velocity. For subsequent intervals, the net flux increment is the flux calculated from the above expression less the flux calculated for the preceding velocity interval and represents only the particles that have lethal mass at the current velocity. In other words,

$$N_{l1} = N_{t1}\ P_1\ ,$$

and for subsequent intervals,

$$N_{li} = [N_{ti} - N_{t(i-1)}]\ P_i\ .$$

All of the lethal flux increments are then summed to provide the total lethal flux, N_{lt}. The summation may be carried out as follows.

$$N_{lt} = (4.266 \times 10^{-15}\ G_e\ E\ t^{-3.445}\ K_1\ \rho_p^{0.575})$$
$$\times \{V_1^{3.014}\ (P_1 - P_2) + V_2^{3.014}\ (P_2 - P_3)$$
$$+ \ . \ . \ . + V_i^{3.014}\ [P_1 - P_{(i+1)}] + \ . \ . \ .$$
$$+ V_{21}^{3.014}\ (P_{21} - P_{22}) + V_{22}^{3.014}\ P_{22}\} \ .$$

The term within brackets, when evaluated from the values given in Table A1, has the value 16754. Substituting this back into the above expression for total lethal flux results in the following.

$$N_{lt} = 7.147 \times 10^{-11}\ G_e\ E\ t^{-3.445}\ K_1^{3.445}\ \rho_p^{0.575} \ . \qquad \text{(Eq. A3)}$$

The probability of impact on the vehicle or on one of its vital components by n or fewer lethal (by virtue of combined mass and velocity) particles during the mission lifetime is determined from the Poisson formula

$$P_{(h \leq n)} = \exp\ (-N_{lt}AT) \sum_{r=0}^{r=n} (N_{lt}AT)^r / r! \ , \qquad \text{(Eq. A4)}$$

where

$P_{(h \leq n)}$ = probability of impact by n or fewer lethal particles,
N_{lt} = lethal particle flux, particles/m^2-s,
A = vehicle or component exposed area, m^2,
T = mission lifetime, s.

Note that the summation term represents the first n + 1 terms of the Maclaurin series that, if carried to an infinite number of terms, equals $\exp(N_{lt}AT)$. Thus, the probability of fewer than an infinite number of lethal particle impacts is 1.0.

One application for Eq. A4 is for the case where a high probability of no lethal impacts on a given component is required. In this case, n = 0, the summation term = 1, and

$$N_{1t}AT = -\ln P_{(h = 0)} \cdot$$

Substituting for N_{1t} from Eq. A3 and solving for the required thickness,

$$t_{(h = 0)} = 1.134 \times 10^{-3} K_1 \rho_p^{0.167} [A T G_e E/-\ln P_{(h = 0)}]^{0.2903} .$$

(Eq. A5)

If, due to redundancy in the design of a component, one or more lethal impacts are tolerable, Eq. A4 may be used to determine the probability that no more than a specified number of penetrations will occur. However, the direct solution for the thickness required to provide a desired probability becomes increasingly difficult as the number of allowable penetrations increases. An iterative method may be used instead, where the value of thickness in Eq. A3 is changed systematically until Eq. A4 yields the desired probability of n or fewer penetrations.

An alternative method that provides a conservative (larger) estimate of the thickness required to provide a desired level of probability that n or fewer penetrations will occur is developed as follows.

As previously noted, Eq. A4 is of the form

$$P = e^{-x} \sum_{r=0}^{r=n} x^r/r! ,$$

where $N_{1t}AT$ is replaced by x and the summation term represents the first n + 1 terms of the Maclaurin infinite series for e^x. The sum of all the remaining terms of the series, R, is as follows.

$$R = e^y x^{(n+1)}/(n+1)! ,$$

where y is not easily determined but lies between 0 and x. The upper bound of R, then, is found by letting y = x or

$$R = e^x x^{(n+1)}/(n+1)! .$$

The general form of the Poisson formula then becomes

$$P \geqq e^{-x}(e^{x} - R)$$

$$\geqq 1 - e^{-x}R$$

$$\geqq 1 - e^{-x}e^{x}x^{(n+1)}/(n+1)!$$

$$\geqq 1 - x^{(n+1)}/(n+1)! \ .$$

Substituting back $N_{1t}AT$ for x,

$$P_{(h \leqq n)} \geqq 1 - (N_{1t}AT)^{(n+1)}/(n+1)! \ .$$

Substituting for N_{1t} as defined in Eq. A3 and solving for the required thickness to provide the desired probability of n or fewer penetrations,

$$t \leqq 1.134 \times 10^{-3} \ K_1 \ \rho_p^{0.167}$$

$$\times \left(\frac{\{[1 - P_{(h \leqq n)}] \ (n+1)!\}^{1/(n+1)}}{G_e \ E \ A \ T} \right)^{-0.2903} \ . \qquad \text{(Eq. A6)}$$

4. APPLICATION OF METHODOLOGY

1. Assume that a space vehicle to be orbited at an altitude of 200 km for 5 years includes a critical component having an exposed area of 10 m^2. The component is fabricated from Nb — 1 Zr (K_1 = 0.34), and a 0.99 probability of zero penetrating meteoroid impacts is desired. A meteoroid density of 0.5 g/cm^3 is assumed. What wall thickness is required to meet this requirement?

$$G_e = 0.568 + 0.432 \times 6378/(6378 + 200)$$

$$= 0.987 \ ,$$

$$E = \left(1 + \cos \{\arcsin [6378/(6378 + 200)]\}\right)/2$$

$$= 0.622 \ .$$

Using Eq. A5,

$$t = 1.134 \times 10^{-3} \times 0.34 \times 0.5^{0.167} \times (10 \times 5 \times 8760 \times 3600 \times 0.978 \times 0.622/-\ln 0.99)e^{0.2903}$$

$$= 0.530 \text{ cm} .$$

2. Assume that a multiple-heat-pipe radiator panel on a vehicle to be orbited at an altitude of 200 km has an exposed vulnerable area of 100 m^2 and is constructed of Nb-1 Zr. Due to redundancy in design, ten of the independent heat pipes can be sacrificed to penetration during the 5-year mission lifetime without impairing mission effectiveness. What tube thickness is required to provide a 0.99 probability that no more than ten penetrations will occur?

Values for G_e, E, and particle density are the same as in the first example. Using Eq. A6 to determine an upper bound for thickness,

$$t \leqq 1.134 \times 10^{-3} \times 0.34 \times 0.5^{0.167} \times \{[(1 - 0.99) \times 11!]^{1/11}/(0.987 \times 0.622 \times 100 \times 5 \times 8760 \times 3600)\}^{-0.2903}$$

$$t \leqq 0.194 \text{ cm} .$$

An iterative solution of Eqs. A3 and A4 yields a required thickness of 0.173 cm, indicating an overestimation of thickness by using Eq. A6 of approximately 12%.

Table A2 presents both the exact solution, using Eqs. A3 and A4, and the approximate solution, using Eq. A6, for the thickness required to provide a 0.99 probability that fewer than up to 30 penetrations will occur during the mission. The magnitude of thickness overestimation by Eq. A6 is indicated by the thickness ratios included in the table. The error increases with number of allowable penetrations, from 12% at 10 lethal hits to 16% at 20 hits and to 19% at 30 hits.

Such an evaluation of required thickness versus degree of design redundancy is a key part of mass optimization of components that can incorporate redundancy through parallel and independent circuitry.

5. CONSIDERATION OF THE DEBRIS PROBLEM

Debris that may impact the vehicle is in an earth orbit having the same altitude as the vehicle at the instant of encounter. If both the vehicle orbit and the debris orbit are circular, the two bodies have identical scalar velocity. Eccentricity in either orbit will cause the scalar velocities to differ from one another. In either case, though, the relative velocity between the two bodies has only a small earth-vertical component and consists primarily of the vector sum of their velocity components normal to earth vertical.

The origin of particles of debris is varied, including material shed by orbiting vehicles and fragments from collisions between orbiting bodies and between orbiting bodies and meteoroids. As a result, their directions of travel within the vehicle's orbital shell are not well defined. However, because many vehicle launches are in an easterly direction, it is likely that much of the debris is traveling as a current with a broadly defined eastward set. Therefore, the likelihood of a purely head-on impact between a debris particle and an orbiting vehicle is low. (An exception is the collision between a vehicle and debris when both are in polar orbit.)

Determination of the probability of the vehicle undergoing no more than some number of penetrating collisions with debris particles during the duration of its mission depends upon knowing the distribution of particle travel directions and the inclination of the vehicle's orbital plane. Because information is lacking on particle direction, and selection of the vehicle orbital plane is based on the intended mission, no general solution is possible at the present. However, a worst case can be hypothesized where the direction of particle travel within the orbital shell is completely random, with as many particles traveling in one direction as in any other direction. An analysis of that case follows.

Defining the direction of particle travel, Θ, as zero when in a direction opposite to that of vehicle travel, the relative velocity between the vehicle and a particle is determined by

$$V_r = \sqrt{2}\, V_0 \sqrt{1 + \cos \Theta} \,,$$

where V_0 is orbital velocity. The impacting, or relative, velocity then varies from 2 V_0 for θ of 0°, to 1.414 V_0 for θ of 90°, to V_0 for θ of 120°, and to zero for θ of 180°. If the debris particles have uniform spatial distribution, the rate of impact by particles traveling in a given direction should be proportional to the relative velocity, V_r, of the particles with respect to the vehicle. This means, unfortunately, that the frequency of impact with particles having high relative velocity, and therefore high damage potential, is higher than for particles having low relative velocity.

Relative velocity and the fraction of total impacts for debris particles traveling in different directions relative to the path of the vehicle are tabulated in Table A3 for an orbital altitude of 200 km (orbital velocity of 7.8 km/s). From these values, the probability distribution of relative velocity given in Table A4 is determined, using velocity increments of 2 km/s.

The debris flux presented in Fig. 4 for the year 2020 is taken to represent the situation for the near future, since indications are that levels predicted for the year 1995 already have been reached. The straight-line portion of the 2020 model can be represented by

$$N_t \text{ (impacts/m}^2\text{-yr)} = 10^{-3.696 - 0.7826 \log m}$$

or

$$N_t \text{ (impacts/m}^2\text{-s)} = 10^{-11.195 - 0.7826 \log m} \quad \text{(Eq. A7)}$$

This equation, combined with Eq. A2 and the velocity probability values from Table A4 in a manner similar to that used in the development of Eq. A3, yield the following expression for the total debris lethal flux.

$$N_{lt} = 8.89 \times 10^{-10}\, t^{-2.223}\, K_1^{2.223}\, \rho_d^{0.371}\,, \quad \text{(Eq. A8)}$$

where

ρ_d = density of debris particle, g/cm³.

The total debris lethal flux is added to the total meteoroid lethal flux as given by Eq. A3 to yield the following expression for the grand total lethal flux from both types of particles.

$$N_{1gt} = 7.147 \times 10^{-11}\, G_e\, E\, t^{-3.445}\, K_1^{3.445}\, \rho_p^{0.575}$$

$$+ 8.89 \times 10^{-10}\, t^{-2.223}\, K_1^{2.223}\, \rho_d^{0.371}\ .$$

Iterative solutions of Eq. A4, after substituting this expression for the grand total lethal flux for N_{1t}, yield thicknesses required to provide a 0.99 probability of no more than various numbers of penetrations during a 5-year mission as shown in Table A5. The density of debris particles was assumed to be 2.7 g/cm^3, corresponding to aluminum.

A modified analysis, assuming that no debris particles are traveling in a direction within 45° of head-on with the vehicle, yielded required thicknesses as given in the the third column of Table A5. It is noteworthy that this rather severe modification to the assumed direction of debris travel results in a reduction in thickness of only 13%.

Comparison of thicknesses given in Table A5, for both the worst-case and the modified assumptions of particle travel, to those in Table A2 indicates that debris particles may be a much greater threat to survivability than meteoroids. Armoring of large areas to such thicknesses as those in Table A5 would be prohibitive from a mass standpoint, making the use of bumpers imperative.

Table A1. Probability-velocity distribution for meteorites

(taken from Fig. 3)

V_{mp}, Midpoint velocity (km/s)	Probability of $V = V_{mp}$	P Probability of $V \geq V_{mp}$
10.5	0.046	1.000
13.5	0.254	0.954
16.5	0.257	0.700
19.5	0.140	0.443
22.5	0.093	0.303
25.5	0.056	0.210
28.5	0.047	0.154
31.5	0.030	0.107
34.5	0.019	0.077
37.5	0.012	0.058
40.5	0.010	0.046
43.5	0.006	0.036
46.5	0.004	0.030
49.5	0.003	0.026
52.5	0.002	0.023
55.5	0.003	0.021
58.5	0.004	0.018
61.5	0.004	0.014
64.5	0.003	0.010
67.5	0.003	0.007
70.5	0.003	0.004
73.5	0.001	0.001

Table A2. Estimated thickness to preclude more than a specified number of penetrating hits[a]

Hits	Thickness (cm) (Eqs. A3, A4)	Thickness (cm) (Eq. A6)	Ratio
0	1.034	1.036	1.002
1	0.473	0.480	1.014
2	0.346	0.357	1.032
3	0.288	0.302	1.048
4	0.253	0.269	1.063
5	0.230	0.247	1.075
6	0.213	0.231	1.086
7	0.200	0.219	1.096
8	0.189	0.209	1.105
9	0.180	0.201	1.113
10	0.173	0.194	1.120
11	0.166	0.188	1.126
12	0.161	0.182	1.132
13	0.156	0.178	1.137
14	0.152	0.173	1.142
15	0.148	0.170	1.147
16	0.144	0.166	1.151
17	0.141	0.163	1.155
18	0.138	0.160	1.159
19	0.135	0.157	1.162
20	0.133	0.155	1.166
21	0.130	0.152	1.169
22	0.128	0.150	1.172
23	0.126	0.148	1.174
24	0.124	0.146	1.177
25	0.122	0.144	1.180
26	0.121	0.143	1.182
27	0.119	0.141	1.184
28	0.118	0.140	1.186
29	0.116	0.138	1.188
30	0.115	0.137	1.190

[a]Target material — Niobium-1 Zr
Orbit altitude — 200 km
Particle density — 0.5 g/cm^3
Target area — 100 m^2
Mission life — 5 years
Probability that number of hits will not be exceeded — 0.99.

Table A3. Relative velocity and fraction of total impacts for debris particles traveling in different directions[a]

Theta[b] degrees	Velocity (km/s)	Fraction of total
0	15.60	0.0427
5	15.59	0.0427
10	15.54	0.0425
15	15.47	0.0423
20	15.36	0.0421
25	15.23	0.0417
30	15.07	0.0412
35	14.88	0.0407
40	14.66	0.0401
45	14.41	0.0395
50	14.14	0.0387
55	13.84	0.0379
60	13.51	0.0370
65	13.16	0.0360
70	12.78	0.0350
75	12.38	0.0339
80	11.95	0.0327
85	11.50	0.0315
90	11.03	0.0302
95	10.54	0.0288
100	10.03	0.0275
105	9.50	0.0260
110	8.95	0.0245
115	8.38	0.0229
120	7.80	0.0214
125	7.20	0.0197
130	6.59	0.0180
135	5.97	0.0163
140	5.34	0.0146
145	4.69	0.0128
150	4.04	0.0111
155	3.38	0.0092
160	2.71	0.0074
165	2.04	0.0056
170	1.36	0.0037
175	0.68	0.0019
180	0.00	0.0000

[a]At orbital altitude of 200 km (orbital velocity = 7.8 km/s).

[b]Theta equals 180° when direction of particle travel is same as vehicle direction of travel.

Table A4. Probability-velocity distribution for debris[a]

V_{mp}, Midpoint velocity (km/s)	Probability of $V = V_{mp}$	Probability of $V \geq V_{mp}$
1	0.006	1.000
3	0.022	0.994
5	0.055	0.972
7	0.059	0.917
9	0.073	0.858
11	0.151	0.785
13	0.180	0.634
15	0.454	0.454

[a]For 2 km/s velocity intervals.

Table A5. Estimated thickness to preclude more than a specified number of penetrating hits by meteoroids and debris[a]

Hits	Thickness[b] (cm)	Modified thickness[c] (cm)
0	10.421	9.030
1	3.105	2.692
2	1.914	1.660
3	1.439	1.248
4	1.181	1.024
5	1.017	0.882
6	0.902	0.783
7	0.817	0.710
8	0.751	0.653
9	0.698	0.607
10	0.655	0.569
11	0.618	0.537
12	0.587	0.510
13	0.559	0.486
14	0.536	0.466
15	0.514	0.447

[a]Target material — Niobium-1 Zr
Orbit altitude — 200 km
Particle density, g/cm^3: meteoroid — 0.5
debris — 2.7
Target area — 100 m^2
Mission life — 5 years
Probability that number of hits will not be exceeded — 0.99.

[b]Assuming uniform distribution of particle travel direction.

[c]Assuming no particles travel in direction within 45° of head-on with the vehicle.

Internal Distribution

1. D. E. Bartine
2. H. I. Bowers
3. D. W. Burton
4. R. H. Cooper
5. W. G. Craddick
6-15. A. P. Fraas
16. H. W. Hoffman
17. R. S. Holcomb
18. D. T. Ingersoll
19. D. B. Lloyd
20-24. J. C. Moyers
25. F. R. Mynatt
26-35. J. P. Nichols
36. H. Postma
37. W. L. Roberts
38. H. E. Trammell
39. K. A. Williams
40. G. L. Yoder
41. ORNL Patent Office
42. Central Research Library
43. Document Reference Section
44-45. Laboratory Records Department
46. Laboratory Records (RC)

External Distribution

47. S. K. Bhattacharyya, Argonne National Laboratory, 9700 S. Cass Avenue, Argonne, IL 60439
48. B. W. Colston, MS F671, Los Alamos National Laboratory, P.O. Box 1663, Los Alamos, NM 87545
49. B. G. Cour-Palais, NASA Johnson Space Center, Code SN3, Houston, TX 77058
50. C. M. Cox, Hanford Engineering Development Laboratory, P.O. Box 1970, Richland, WA 99352
51. L. Cropp, Sandia National Laboratories, P.O. Box 5800, Albuquerque, NM 87185
52. P. Dirkmaat, DOE-ID, 550 Second Street, Idaho Falls, ID 83274
53. R. E. English, NASA Lewis Research Center, MS 501-15, 21000 Brookpark Road, Cleveland, OH 44135
54. D. H. Humes, NASA Langley Research Center, MS 160, Hampton, VA 23665-5225
55. D. J. Kessler, NASA Johnson Space Center, Code SN3, Houston, TX 77058
56. E. U. Khan, U.S. Dept. of Energy, NE-54, Germantown, Washington, D.C. 20545
57. J. Loria, NASA Headquarters, 400 Maryland Avenue SW, Washington, D.C. 20546
58. E. T. Mahefkey, Jr., Aero Propulsion Laboratory (POOC-5), U.S. Air Force Wright Aeronautical Laboratories, Wright-Patterson Air Force Base, OH 45433
59. J. R. Powell, Brookhaven National Laboratory, Associated Universities, Inc., Upton, NY 11973
60. J. M. Smith, NASA Lewis Research Center, MS 500-202, Building 4013, 21000 Brookpark Road, Cleveland, OH 44135
61. R. J. Sovie, NASA Lewis Research Center, MS 500-202, Building 4013, 21000 Brookpark Road, Cleveland, OH 44135
62. R. Verga, Strategic Defense Initiative/Director of Energy, The Pentagon, Washington, D.C. 20301-7100
63. E. J. Wahlquist, U.S. Dept. of Energy, NE-54, Germantown, Washington, D.C. 20545

64. C. E. Walter, Lawrence Livermore National Laboratory, University of California, P.O. Box 808, Livermore, CA 94550
65. R. D. Widrig, Pacific Northwest Laboratory, Battelle Boulevard, Richland, WA 99532
66. G. R. Woodcock, Boeing Aerospace Company, Post Office Box 1470, Huntsville, AL 35807
67. R. Wylie, Strategic Defense Initiative/Director of Energy, The Pentagon, Washington, D.C. 20301-7100
68. H. R. Zweig, Energy Technology Engineering Center, Rocketdyne Division, Rockwell International Corp., P.O. Box 1449, Canoga Park, CA 91304
69. Office of Assistant Manager for Energy, Research and Development, DOE-Oak Ridge Operations, Oak Ridge, TN 37831

70-96. Office of Scientific and Technical Information, P.O. Box 62, Oak Ridge, TN 378319